https://doi.org/10.5194/egusphere-2023-539
Preprint. Discussion started: 27 March 2023

Investigating the contribution of grown new particles to cloud condensation nuclei with largely varying pre-existing particles - Part 1: Observational data analysis

Xing Wei[1#], Yanjie Shen[1,2#], Xiao-Ying Yu[3*], Yang Gao[1,4], Huiwang Gao[1,4], Ming Chu[1], Yujiao Zhu[5], Xiaohong Yao[1,4,6*]

[1]Key Laboratory of Marine Environment and Ecology (MoE) and Frontiers Sci Ctr Deep Ocean Multispheres & Earth, Ocean University of China, Qingdao, China

[2]College of Biology and Oceanography, Weifang University, Weifang, China

[3]Materials Science and Technology Division, Oak Ridge National Laboratory, Oak Ridge, TN 37831-6136, USA

[4]Laboratory for Marine Ecology and Environmental Sciences, Qingdao National Laboratory for Marine Science and Technology, Qingdao, China

[5]Environment Research Institute, Shandong University, Qingdao 266237, China

[6]Sanya Oceanographic Institution (Ocean University of China), Yazhou Bay Science & Technology City, Sanya, China

#Equally contributed to the study; ***Correspondence to***: Xiao-Ying Yu (yuxiaoying@ornl.gov) and Xiaohong Yao (xhyao@ouc.edu.cn)

Abstract. This study employed multiple techniques to investigate the contribution of grown new particles to the number concentration of cloud condensation nuclei (CCN) at various supersaturation (SS) levels at a rural mountain site in North China Plain from 29 June to 14 July 2019. On eight new particle formation (NPF) days, the total particle number concentrations (N_{cn}) were 8.4±6.1 ×10^3 cm^{-3}, which were substantially higher compared to 4.7±2.6 ×10^3 cm^{-3} on non-NPF days. However, the N_{ccn} at 0.2 %SS and 0.4 %SS on the NPF days were significantly lower than those observed on non-NPF days ($P<0.05$). This was due to the lower cloud activation efficiency of pre-existing particles resulting from organic vapor condensation and smaller number concentrations of pre-existing particles on NPF days. A case-by-case examination showed that the grown new particles only yielded a detectable contribution to N_{ccn} at 0.4 % SS and 1.0 % SS during the NPF event on 1 July 2019, accounting for 12±11 % and 23±12 % of N_{ccn}, respectively. The increased N_{ccn} during two other NPF events and at 0.2 % SS on 1 July 2019 were detectable, but determined mainly by varying pre-existing particles rather than grown new particles. In addition, the hygroscopicity parameter values, concentrations of inorganic and organic particulate components, and surface chemical composition of different sized particles were analyzed in terms of chemical drivers to grow new particles. The results showed that the grown new particles via organic vapor condensation generally had no detectable contribution to N_{ccn}, but incidentally did. However, this conclusion was drawn from a small size of observational data, leaving more observations, particularly for long-term observations and the growth of pre-existing particles to the CCN required size, needed for further investigation.

Keywords: New particles; pre-existing particles; cloud condensation nuclei; hygroscopicity parameter; ammonium nitrate.

https://doi.org/10.5194/egusphere-2023-539
Preprint. Discussion started: 27 March 2023

1 Introduction

Global warming and climate change have become significant topics of discussion and debate in recent decades (IPCC, 2021). Atmospheric aerosols, activated as cloud condensation nuclei (CCN) at super saturation (SS) conditions, can form cloud droplets and provide substantial global cooling, subsequently alleviating warming (Twohy 2005; Dusek et al., 2006; Small et al., 2009; Kerminen et al., 2012, 2018; Sullivan et al., 2018; Zaveri et al., 2021; Yu et al., 2020). However, compared to other climate forcing factors, aerosol-cloud interactions remain the largest uncertainty (IPCC, 2021). The CCN may act as one of the key contributors to this uncertainty, considering their roles in increasing the number concentration of cloud droplets and decreasing the size of cloud droplets (Twomey et al., 1977; Albrecht, 1989; Andreae and Rosenfeld, 2008; Bulgin et al., 2008). To minimize the large uncertainty on aerosol-cloud interactions, significant efforts have been made to improve the understanding of CCN regarding their primary and secondary sources, and aerosol activation properties in different size ranges with varying SS from the polluted atmosphere to the remote clean atmosphere (Yu and Luo, 2009; Kerminen et al., 2012, 2018; Li et al., 2017a; Williamson et al., 2019; Zhu et al., 2019a; Zaveri et al., 2021, Iwamoto et al., 2021).

New particle formation (NPF) refers to the phenomenon of gas-particle nucleation followed by the growth of newly formed particles in the atmosphere. During an NPF event, particle number concentrations (PNCs) can rapidly increase in different size ranges (Kulmala et al., 2004; Chu et al., 2019; Lee et al., 2019). The grown new particles, defined as particles larger than 5.6 nm (the size detection limit of a particle sizer used for sampling in this study), have been reported to contribute to the CCN budget according to field measurements and modeling studies (Kuang et al., 2009; Kerminen et al., 2012; Ehn et al., 2014; Kalivitis et al., 2015; Leng et al., 2014; Ma et al., 2016; Tröstl et al., 2016; Gordon et al., 2017; Li et al., 2017b; Williamson et al., 2019; Fang et al., 2021; Sebastian et al., 2021). However, field studies are often affected by perturbations associated with varying pre-existing particles in PNCs, size spectra, and cloud activation properties. As a result, observational evidence on the net contribution of the grown new particles to CCN concentrations is limited, particularly at low ambient SS, i.e., SS < 0.2–0.3 % (Kerminen et al., 2012; Tröstl et al., 2016; Rose et al., 2017; Sebastian et al., 2021).

Organic vapors have been found to play a dominant role in the growth of newly formed particles, ranging from a few nanometers to submicron scales (Pierce et al., 2012; Wu et al., 2013; Ehn et al., 2014; Kalivitis et al., 2015; Kawana et al., 2017; Ma et al., 2021; Wan et al., 2020; Chang et al., 2022). This organic-driven growth may reduce the Kelvin effect for water vapor condensation on small-sized particles (Dusek et al., 2006), while the condensation of low-volatile organic vapors on grown new particles and pre-existing particles can decrease the aerosol hygroscopicity due to their low hygroscopicity parameter (κ) values that approach 0.1 (Petters and Kreidenweis, 2007; Dusek et al., 2010; Wu et al., 2013; Zhu et al., 2019b; Fang et al., 2021; Chang et al., 2022). However, some semi-volatile organic species, such as oxalic acid, have been found to have high cloud activation potentials, with a κ value of 0.81, and their neutralized salts also have κ values of 0.59–0.70 (Boreddy and Kawamura, 2018). Additionally, secondary organic aerosols (SOA) from dark ozonolysis of γ-terpinene under different reaction conditions have shown moderate cloud activation potentials, with κ values of 0.20–0.24 (Bouzidi et al, 2022). The κ values of pre-existing particles vary in different environments, with the global average

https://doi.org/10.5194/egusphere-2023-539
Preprint. Discussion started: 27 March 2023

around 0.27 (Petters and Kreidenweis, 2007; Kerminen et al., 2012). During an NPF event, when different organic vapors condense simultaneously on grown new particles and pre-existing particles, the κ values of different sized particles can either decrease, increase, or remain invariant, leading to corresponding changes in CCN concentrations. Therefore, statistical analysis is essential in understanding the complex interactions between organic vapors and particle hygroscopicity, which is currently scarce in the literature.

Various studies have reported that sulfuric acid vapor generated from photochemical reactions in the atmosphere contributes to the growth of newly formed particles (Birmili et al., 2003; Boy et al., 2005; Yue et al., 2011, Bzdek et al., 2012, Vakkari et al., 2015; Ma et al., 2016; Fang et al., 2021). However, the contribution of sulfuric acid vapor to growing secondary particles from 40–50 nm to larger sizes is highly questionable, as observed subsequent growth often occurs at nighttime (Man et al., 2015; Ma et al., 2021). Furthermore, the relative contribution of ammonium nitrate (NH_4NO_3), one of the most important components in atmospheric particles, increases with a faster decrease in SO_2 emissions globally (Chan and Yao, 2008; Cao et al., 2017; Ge et al., 2017; Rodelas et al., 2019; Wu et al., 2019; Bressi et al., 2021; Zhu et al., 2021). Current modeling studies suggest the importance of NH_4NO_3 aerosols in regional cooling (Drugé et al., 2019; Jones et al., 2021). Our previous studies have found that the formation of particulate NH_4NO_3 via HNO_3 and NH_3 gases plays a key role in the second-phase growth of newly formed particles from 40–50 nm to larger sizes at nighttime without photochemical reactions (Zhu et al., 2014; Man et al., 2015; Ma et al., 2021). Recently, Wang, M. et al. (2020) proposed rapid particle formation and growth of newly formed particles by NH_4NO_3 formation. Unlike organic vapors, NH_4NO_3 formation on newly formed particles and pre-existing particles should always yield a net increase in CCN concentrations during NPF events. However, to the best of our knowledge, no field studies have reported this phenomenon.

The objective of this study is to investigate the relationship between newly formed particles and CCN using particle number size distributions (PNSDs), CCN concentrations, and the derived κ values of atmospheric aerosols at various SS. Chemical composition of atmospheric particles was also analyzed by multiple techniques to support the analysis. The observations were conducted at a rural mountain site (1100 m above sea level) in North China Plain (NCP) from June to July in 2019, during the rainy season when morning mist frequently occurred among mountain peaks. The observed CCN were directly related to the formation of cloud droplets at the elevated mountain site. Three scientific questions were addressed: (1) Does the organic-driven growth of newly formed particles contribute to the observed CCN at various SS? Is the effect of organic condensation reduced on pre-existing particles during NPF events? (2) What is the relative role of organic condensation and NH_4NO_3 formation in determining the contribution of grown new particles to the observed CCN at various SS? (3) What implications do our findings have on knowledge gaps for CCN sources in NCP? In a companion paper, a modeling study is applied to illustrate the link in three dimensions and quantify the contributions of different chemical species to the growth of newly formed particles (Chu et al., 2023).

https://doi.org/10.5194/egusphere-2023-539
Preprint. Discussion started: 27 March 2023

2 Experimental

2.1 Sampling period and site

A research campaign was performed from 23 June to 14 July 2019 at a mountain site (115°26′E, 39°58′N) in western Beijing to investigate the CCN activation of atmospheric aerosols in the rural atmosphere over the North China Plain (NCP). The sampling site, located at an altitude of approximately 1100 m (Fig. 1a–f), belongs to a forest ecosystem research station of the Chinese Academy of Science. The mountain site is surrounded by secondary forests and is approximately 110 km southwest downwind from Beijing. NO_2 column densities during the study period showed that anthropogenic combustion emission sources were mainly distributed in the east and south of the site (Fig. 1a–f), while the north and west directions frequently displayed lower NO_2 column densities, indicating a cleaner rural environment.

2.2 Particle collection

Four different instruments were installed on the third floor of the station major building, at a height of 10 m above ground. These instruments include a Fast Mobility Particle Sizer (FMPS, TSI, 3091) downstream of a dryer (TSI, 3062), a Condensation Particle Counter (CPC, TSI, 3775), a continuous flow CCN counter (CCNC, DMT Model 100), and a Differential Mobility Analyzer (DMA, Grimm) coupled with a Nanometer Aerosol Sampler (NAS, Grimm). The FMPS was used to measure particle concentrations in the size range of 5.6 nm to 560 nm in 32 channels at a frequency of 1 Hz. For the purpose of this study, the total particle number concentration (total N_{cn}) and number concentrations of particles larger than 100 nm ($N_{cn>100}$) were defined as the sum of number concentrations from 5.6 nm to 560 nm and >100 nm to 560 nm, respectively. The CPC shared a spitter with the FMPS and generated data at a 2 s time resolution to correct the FMPS data (Zimmerman et al., 2015). The CCNC was used to measure the bulk CCN concentration (N_{ccn}) at five different supersaturation (SS) levels of 0.2 %, 0.4 %, 0.6 %, 0.8 %, and 1.0 %. Further details about these instruments can be found in Li et al. (2015), Wang et al. (2019), and Gao et al. (2020). The CCNC was operated properly from 29 June 2019, and thus measurements analyzed in this study were taken from 29 June to 14 July 2019.

The DMA coupled with the NAS was used to collect atmospheric nanoparticles at four diameters: 30 nm, 60 nm, 100 nm, and 200 nm. The DMA initially separated atmospheric particles, which were then collected on Transmission Electron Microscopy (TEM) grids (01814-F, TED PELLA, INC.) by the NAS using electrostatic force. To ensure that sufficient particles were collected for chemical analysis, each sample was collected for 2 hours, with a sampling rate of 1 L/min and a sheath flow rate of 10 L/min. A total of 14 sample sets and three field blanks were collected. The chemical composition of the samples collected on 30 June and 1 July 2019 was successfully analyzed. Additionally, field blanks were analyzed to identify interference peaks from substrates.

11 total suspended particle (TSP) samples were collected during the campaign on quartz filters using a high-volume sampler operating at a flow rate of approximately 1 m^3/min. The collected samples were utilized for analyzing inorganic ions, organic carbon (OC), elemental carbon (EC), and organic tracers. The sampling duration of each sample was around 24 hours, which ensured sufficient particle loading for multiple chemical analyses. Additionally, meteorological data such as wind speed (WS), wind

https://doi.org/10.5194/egusphere-2023-539
Preprint. Discussion started: 27 March 2023

direction (WD), ambient temperature (T), and relative humidity (RH) were continuously measured at a height of 10 m above ground level at the station.

2.3 Chemical analysis of particles

A ToF-SIMS (time-of-flight secondary ion mass spectrometer) instrument (IONTOF V, IONTOF GmbH, Münster, Germany) was utilized to analyze the chemical composition of atmospheric nanoparticles collected using the DMA coupled with NAS at four different sizes. During analysis, the main chamber pressure was kept under a vacuum of 10^{-8} mbar. The primary ion beam was Bi^{3+} (25 keV) with 10 kHz pulse energy, a pulse width of 0.8 ns, and a current set at approximately 0.6 pA. The SIMS spectra were acquired over an area of 150×150 μm^2 for 60 scans, with at least 4 positive and 4 negative data points collected for each sample. The IONTOF Surface Lab 6.3 software was used for SIMS data analysis. The mass spectra were calibrated using m/z^+ 15 CH_3^+, 55 $C_4H_7^+$, and 91 $C_7H_7^+$ in the positive ion mode, and m/z^- 26 CN^-, 41 C_2HO^-, and 77 CHO_4^- in the negative ion mode, respectively. Principal component analysis (PCA) was conducted using MATLAB software to study the differences in chemical composition among the selected-size particles. Prior to conducting spectral PCA, the interference peaks from substances were deleted, and the mass-calibrated data were treated by mean-centering, normalization to the total ion intensity of all selected peaks, and square-root transformation (Ding et al., 2016, 2019; Zhang et al., 2019; Sui et al., 2017; Fu et al., 2018; Cheng et al., 2014).

For the analysis of TSP samples, a 1/4 fraction of each filter was utilized to measure organic tracers using gas chromatography mass spectroscopy (GC-MS) with an Agilent 6890 GC/5975 MSD, as described in previous studies (Kleindienst et al., 2007; Feng et al., 2013). The OC and EC concentrations were analyzed using a thermal/optical carbon analyzer (DRI 2001A, Atmoslytic Inc., USA) with the IMPROVE temperature program. First, the OC was volatilized under helium by heating the filter to 580 ℃ in four steps and then to 870 ℃ in three steps in a He:O_2 environment. The charring of OC was monitored using a He-Ne laser of 650 nm. The secondary OC (SOC) was estimated as (OC–2×EC) following the method of Yu et al. (2009). Inorganic and organic ions were analyzed using ion chromatography (Dionex 3000) from a 1/4 fraction of each TSP sample filter, as detailed in the supporting information (Hu et al., 2015; Teng et al., 2017). More experimental details can be found in the supporting information.

2.4 Definition of NPF events and calculation methods

NPF events were identified using the criteria proposed by Dal Maso et al. (2005) and Kulmala et al. (2012), which require the observation of new nucleation mode particles in the spectra and their prevalence or growth over several hours. These criteria distinguish NPF particles from plume and pre-existing particles. NPF events were considered to have ended when the new particle signals disappeared, and the total particle number concentration returned to the background levels before the NPF events or when the newly formed particles were suddenly overwhelmed by plumes and could no longer be identified. NPF days (non-NPF days) were defined as the presence (absence) of NPF events. Two metrics, the apparent formation rate (FR) and the net maximum increase in the nucleation mode number concentration (NMINP), were used to quantify the intensity of NPF events (Sihto et al., 2006; Kulmala et al., 2012; Zhu et al, 2021). FR and NNIMP during the NPF events were calculated based on the

https://doi.org/10.5194/egusphere-2023-539
Preprint. Discussion started: 27 March 2023

nucleation mode particles in the size range of 5.6 to 30 nm. Particle number size distributions (PNSDs) in this study were fitted using multi-lognormal distribution functions (Whitby, 1978; Yao et al., 2005), and the calculation methods are described in detail in the Supporting Information.

The κ was calculated in equation (1) that proposed by Petters and Kreidenweis (2007):

$$\kappa=\frac{4A^3}{27D_d^3\ln^2S_C},\ A=\frac{4\sigma_{s/a}M_w}{RT\rho_w} \quad (1)$$

where D_d is the particle dry diameter, and it was assumed to be equal to the critical diameter for CCN activation (D_{crit}). S_C is the supersaturation. $\sigma_{s/a}$ is set as 0.0072 J m^{-2}, representing the surface tension over the interface of solution and air, M_w is the molecular of water, R is the universal gas constant, T is temperature, and ρ_w is water density. In this study, the hourly κ values at 0.2 %, 0.4 % and 1.0 % SS were calculated for analysis. D_{crit} is defined as the particle diameter which is considered as the lower limit of the integral on particle number, and the upper limit was set as the largest particle diameter, yielding the total integrated particle number concentration equal to the CCN concentration (Hung et al., 2014; Cheung et al., 2020; Gao et al., 2020). The calculated hourly κ values reflect the overall effect on particle size, chemical composition, and mixing state, which are thereby referred to as the bulk κ values under different SS conditions.

Satellite products do not provide accurate retrievals of cloud droplet number concentration (CDNC) due to uncertainties introduced by lidar-derived biases. Building on the "adiabatic cloud model" assumption (Bennartz, 2007; Bennartz and Rausch, 2017), an effective computational method is established to estimate liquid-phase CDNCs based on cloud optical thickness and cloud effective radius in eqn. (2) and (3):

$$CDNC=\frac{\tau^3}{k}[2W]^{\frac{5}{2}}[\frac{3}{5}\pi Q]^{-3}[\frac{3}{4\pi\rho_w}]^{-2}c_w^{\frac{1}{2}} \quad (2)$$

$$W=\frac{5}{9}\rho_w\tau r_e \quad (3)$$

where τ is cloud optical thickness (COT), k equal to 0.8 presents the dispersion of the assumed cloud droplet size distribution, Q is approximately 2 as the scattering efficiency of droplet, c_w is the condensation rate and it is calculated following previous studies (Ahmad et al., 2013; Grosvenor et al., 2018; Li et al., 2018). W is liquid water path (LWP), and r_e is cloud effective radius (CER). COT and CER were derived from daily mean level-3 daily 1° cloud retrieval product (MYD08_D3) retrieved from Aqua-MODIS and the dataset from June 2019 to July 2019.

We modeled air mass back trajectories at 1000 m by using the Hybrid Single-Particle Lagrangian Integrated Trajectory (HYSPLIT) model from the NOAA Air Resources Laboratory. Simulations were performed every 2 hours starting from 2 hours before the NPF and ended until the NPF signals disappeared (Fig. 1a–f). NO_2 column densities were downloaded from https://so2.gsfc.nasa.gov/no2/no2_index.html.

https://doi.org/10.5194/egusphere-2023-539
Preprint. Discussion started: 27 March 2023

3 Results and discussion

3.1 Overview of the measured N_{ccn} related to NPF events

Figure 2a showed the hourly average N_{ccn} at 0.2 %, 0.4 %, and 1.0 % SS and the 1-min average total N_{cn} from 29 June to 14 July 2019, respectively. Table S1 provides the daily average N_{ccn} (average ± standard deviation) at SS values ranging from 0.2 % to 1.0 %, the daily average $N_{cn>100}$, and the total N_{cn}. The N_{ccn} varied by approximately one order of magnitude, ranging from 0.10 $\times 10^3$ cm^{-3} to 4.7 $\times 10^3$ cm^{-3} (1.4±0.7 $\times 10^3$ cm^{-3}) at 0.2 % SS and from 0.10 $\times 10^3$ cm^{-3} to 4.8 $\times 10^3$ cm^{-3} (1.7±0.9 $\times 10^3$ cm^{-3}) at 0.4 % SS. The temporal trend in N_{ccn} at 1.0 % SS was consistent with those at 0.2 % and 0.4 % SS, while the values of N_{ccn} at 1.0 % SS were 2.2±1.1 $\times 10^3$ cm^{-3}, which was approximately 60 % higher than that at 0.2 % SS. The N_{ccn} values observed on 29–30 June 2019 were 0.69±0.27 $\times 10^3$ cm^{-3}, 0.83±0.36 $\times 10^3$ cm^{-3}, and 1.2±0.6 $\times 10^3$ cm^{-3} at 0.2 %, 0.4 %, and 1.0 % SS, respectively. These values decreased by approximately 50 % relative to the campaign averages observed during the 16 days. However, the total N_{cn} on those 2 days ranked at a moderately high level (see Table S1), implying lower cloud activation potentials of the observed aerosols. Although no size-dependent chemical components were measured, the calculated ratios of SOC/(SO_4^{2-}+NO_3^-) in TSP on those 2 days were substantially larger than those from other days (see Fig. 2b), implying that the larger fraction of organics prevented aerosols from being activated as CCN (Petters and Kreidensohler, 2007; Kawana et al., 2017; Zhu et al., 2019b; Crumeyrolle et al., 2021; Chang et al., 2022). Surprisingly, the satellite-derived CDNC of 341–386 cm^{-3} over the mountain area were higher on those 2 days (see Fig. 2c). On the other 14 days, the CDNC were determined to be 106±55 cm^{-3}, approximately one order of magnitude smaller than the observed corresponding to N_{ccn} at 0.2 % SS. The observed N_{ccn} appeared to be sufficient to form cloud droplets, although N_{ccn} may decrease to some extent from 1000 m to higher heights (Li et al., 2019; Yang et al., 2020; Che et al., 2021).

Compared to observations at 0.2 % SS reported in the literature, the campaign average N_{ccn} during the 16 days in this study was almost double the value of 0.8±0.7 $\times 10^3$ cm^{-3} measured during 3 weeks of summer in 2014 on Mt. Huang (Anhui province, China) (Miao et al., 2015). However, the average N_{ccn} was only half of that observed at a suburban site of Qingdao (Shandong province, China) in the spring of 2013 (Li et al., 2015). At 0.4 % SS, the average N_{ccn} during the 16 days was also double the values observed at SMEAR II station (a rural forest site) in Hyytiälä in July 2008 and June 2009 (Sihto et al., 2011), and substantially larger than the values of 166–700 cm^{-3} at 0.11–0.80 % SS over a mid-latitude forest in Japan (Deng et al., 2018). Assuming that the rural atmospheric observations reported in the literature represent upper limits for natural contributions, it is likely that at least 50 % of the observed N_{ccn} in this study were derived from primary and secondary anthropogenic aerosols. However, the measured concentrations of EC in TSP were only 0.23–0.53 μg m^{-3} in this study (See Table 1), consistent with values of 0.10–0.43 μg m^{-3} in $PM_{2.5}$ in remote atmospheres across North America (Ahangar et al., 2021). Given the low CCN activation of primary aerosols (Gao et al., 2020), it is expected that secondary anthropogenic aerosols contributed significantly to N_{ccn} (Ma et al., 2021) and were therefore investigated below.

Nucleation events have been identified as significant sources of atmospheric particles in terms of

https://doi.org/10.5194/egusphere-2023-539
Preprint. Discussion started: 27 March 2023

number concentration (Kulmala et al., 2004; Chu et al., 2019; Lee et al., 2019). In this study, such events were observed frequently on 8 out of the total 16 days (Figs. 3–5 and Fig. S1), with air masses mainly originating from the northwest, north, and northeast during these events (Fig. 1a–f). Shorter air mass back trajectories were obtained from 12 July to 14 July, and shorter durations of nucleation events were observed. As shown in Table S1, significantly lower N_{ccn} values were observed on nucleation days compared to non-nucleation days (with $P<0.05$), namely, $1.2\pm0.7 \times10^3$ cm^{-3} on nucleation days versus $1.6\pm0.8 \times10^3$ cm^{-3} on non-nucleation days at 0.2 % SS. The same trend was observed at 0.4 % SS, with the values of $1.5\pm0.9 \times10^3$ cm^{-3} on nucleation days and $1.8\pm0.9 \times10^3$ cm^{-3} on non-nucleation days, respectively. However, the N_{ccn} values at 1.0 % SS on nucleation days ($2.1\pm1.2 \times10^3$ cm^{-3}) did not differ significantly from those observed on non-nucleation days ($2.3\pm1.1 \times10^3$ cm^{-3}) ($P>0.05$). Hirshorn et al. (2022) analyzed 15 years of observational data from mountaintop location in North America and found that N_{ccn} did not show a significant increase during NPF events in either summer or autumn. Kawana et al. (2017) also reported lower mean N_{ccn} values on nucleation days compared to non-nucleation days at a forest site in Wakayama (Japan) during the summer, which were likely due to biogenic secondary organic condensation on atmospheric particles. Theoretically, newly formed particles may continue to grow even after the new particle signal disappears from observations. However, larger and smaller pre-existing particle growth was observed only on 4 July (1 of 16 days), from 88 nm to 116 nm and from 24 nm to 32 nm, respectively (See Fig. S2), indicating that the occurrence of pre-existing particle growth was infrequent. Moreover, the growth of newly formed particles extended to the next day, occurring only during one nucleation event, where newly formed particles grew from 1 July to the early morning of 2 July. Therefore, the observations on 2 July were reclassified as nucleation days and removed from non-nucleation days. The re-calculated N_{ccn} values on nucleation days did not differ significantly from those on non-nucleation days at SS=0.2 % and 0.4 % with $P>0.05$, namely, $1.3\pm0.5 \times10^3$ cm^{-3} (nucleation days) versus $1.4\pm0.5 \times10^3$ cm^{-3} (non-nucleation days) at 0.2 % SS, and $1.6\pm0.7 \times10^3$ cm^{-3} (nucleation days) versus $1.6\pm0.6 \times10^3$ cm^{-3} (non-nucleation days) at 0.4 % SS. The change suggested that the significance of the N_{ccn} discrepancy between nucleation and non-nucleation days at 0.2 % and 0.4 % SS was sensitive to the applied data size. However, further investigation through long-term observations is required to determine whether nucleation events can contribute to a statistically significant increase in CCN concentration.

Excluding 2 July, the $N_{cn>100}$ on NPF days were significantly lower at ($1.6\pm0.8 \times10^3$ cm^{-3}) compared to non-NPF days ($1.8\pm1.0 \times10^3$ cm^{-3}) with $P<0.05$ (Table S1), which partially explained the lower N_{ccn} at 0.2 % SS. However, the total N_{cn} substantially increased on NPF days to $8.4\pm6.1 \times10^3$ cm^{-3} compared to $4.7\pm2.6 \times10^3$ cm^{-3} on non-NPF days. During the first 2–3 hours of the NPF events, the total N_{cn} increased significantly from $4.2\pm1.1 \times10^3$ to $21\pm5.4 \times10^3$ cm^{-3} with the NMINP of $17\pm6.0 \times10^3$ cm^{-3} (Fig. 2a). Nonetheless, the increase in the total N_{cn} did not result in a statistically significant increase in the observed N_{ccn} at SS from 0.2 % to 1.0 % on NPF days compared to non-NPF days, regardless of including or excluding 2 July from NPF days. It is important to note that the observational data alone cannot provide evidence of any additional evolution of new particles after the new particle signal disappears, particularly considering the infrequent occurrence of the pre-existing particle growth. Therefore, the same is true for the related contribution to N_{ccn}.

https://doi.org/10.5194/egusphere-2023-539
Preprint. Discussion started: 27 March 2023

The statistical comparisons between NPF and non-NPF days in this study showed contradictory results to those previously reported in the literature. In other words, the findings of this study contradicted the idea that NPF events are important secondary sources of CCN, which has been reported in previous studies (Sotiropoulou et al., 2006; Kuwata et al., 2008; Wiedensohler et al., 2009; Sihto et al., 2011; Ma et al., 2016; Rose et al., 2017; Kerminen et al., 2018; Wang Y., et al., 2020; Fang et al., 2021; Chang et al., 2022). Therefore, this paper presents a case-by-case examination from Sect. 3.2 to Sect. 3.5 where the contributions of NPF events to the N_{ccn} are elaborated at various SS. Section 3.2 presents the analysis results of five NPF events on 29 June, 3 and 12–14 July. The NPF events did not cause an increase in N_{ccn} at 0.2 %, 0.4 %, and 1.0 % SS (See Fig. 3 and Fig. S1). Section 3.3 includes two NPF events on 30 June and 6 July when an increase in N_{ccn} was indeed observed (See Fig. 4). However, this increase was associated mainly with changing number concentrations and/or κ values of pre-existing particles. On 1 July, an increase in N_{ccn} was observed during the NPF event (See Fig. 5), while the grown new particles unlikely contributed to N_{ccn} at 0.2 % SS. The results are analyzed in Sect. 3.4. When the N_{ccn} at 0.4 % and 1.0 % SS were analyzed in the NPF event on 1 July, the contributions of the grown new particles to N_{ccn} could be reasonably qualified at nighttime with a large increase in κ values of atmospheric particles. These results are presented in Sect. 3.5.

3.2 Case study with no detectable contribution to N_{ccn} during NPF events

Figure 3a–f shows that there was no detectable contribution of grown new particles to N_{ccn} in the NPF events on 29 June and 3 July. Specifically, higher values of N_{ccn} at 0.2 % and 0.4 % SS were observed before 06:00 (24 hours used here and afterwards) on 29 June, which were associated with the intrusion of aerosol plumes and higher κ values of 0.33±0.06 at 0.2 % SS and 0.16±0.03 at 0.4 % SS (see Fig. 3a–c). The κ values at 0.2 % SS were close to the global average values and those reported in suburban or rural polluted atmospheres of China (Petters and Kreidensohler, 2007; Rose et al., 2010, 2011; Ma et al., 2016; Fang et al., 2021). Assuming that the activated aerosols at 0.2 % SS were internally mixed and mainly composed of inorganic ammonium salts and organics (Petters and Kreidensohler, 2007; Rose et al., 2010, 2011), they would contribute almost equally to the total mass concentration of the associated aerosols. The κ values of 0.16±0.03 at 0.4 % SS were also reported in remote forest or less polluted areas (Gunthe et al., 2009; Dusek et al., 2010; Cerully et al., 2011; Sihto et al., 2011; Levin et al., 2014; Kawana et al., 2017; Fang et al., 2021; Park et al., 2021). The calculated κ values almost halved with SS increasing from 0.2 % to 0.4 % before 06:00, suggesting that the observed aerosols in smaller sizes had lower cloud activation potentials. Similar results were frequently reported in the literature, i.e., the fraction of organics in atmospheric nanometer particles increased with the decrease of particle sizes (Rose et al., 2010, 2011; Crippa et al., 2014; Cai et al., 2017). After 06:00, the calculated κ values at 0.2 % and 0.4 % SS largely decreased to be less than 0.1. The low κ values suggested that atmospheric aerosols measured after 06:00 mainly consisted of low CCN-activated organics (Petters and Kreidensohler, 2007; Kerminen et al., 2018; Chang et al., 2022).

On 29 June, the NPF became noticeable at 08:35, causing the total N_{cn} to increase rapidly by over one order of magnitude within 2 hours with a FR of 2.3 cm^{-3} s^{-1} and NMINP of 2.0 $\times 10^4$ cm^{-3}. The newly formed particles took approximately 3 hours to grow from the initial median mode diameter of <10 nm

https://doi.org/10.5194/egusphere-2023-539
Preprint. Discussion started: 27 March 2023

to the maximum median mode diameter of 19±1 nm. However, similar to our previous findings and other studies reviewed by Chu et al. (2019), new particles stopped growing after approximately 10 hours and could even slightly shrink before disappearing. With κ values <0.1, only atmospheric particles larger than 120–200 nm could be activated as CCN at 0.2 % and 0.4 % SS (Petters and Kreidensohler, 2007), which is conventionally referred to as the CCN-activated size. Even at 1.0 % SS, the CCN-activated size at κ values <0.1 (Fig. S3) should be larger than 70 nm. Therefore, the newly grown particles were too small to act as CCN, regardless of ambient SS, as previously reported (Hammer et al., 2014; Hudson et al., 2015; Shen et al., 2018). Moreover, the variations in N_{ccn} at 0.2 % SS were likely determined by the number concentrations of larger pre-existing particles based on the correlation between N_{ccn} at 0.2 % SS and $N_{cn>100}$ from 09:00 to 24:00 on 29 June. The regression equation can be expressed as follows: $N_{ccn} = N_{cn>100} \times 0.42 + 64$, with an R^2 of 0.70 and $P<0.01$, at 0.2 % SS.

On 3 July, NPF event commenced at 08:10 with FR of 0.75 cm^{-3} s^{-1} and NMINP of 9.5 $\times 10^3$ cm^{-3} s^{-1} (refer to Fig. 3d–f). However, between 06:00 to 13:00, the N_{ccn} at 0.2 % and 0.4 % SS decreased with decreasing κ values. Meanwhile, $N_{cn>100}$ slightly increased during the same time period. It is likely that less CCN-activated vapor condensation had a significant effect on the growth of pre-existing particles resulting in the increase of $N_{cn>100}$ and decrease of N_{ccn}. Following 13:00, N_{ccn} values at 0.2 % and 0.4 % SS experienced two stepwise increases, accompanied by an increase in $N_{cn>100}$. For example, N_{ccn} values at 0.2 % and 0.4 % SS almost doubled with the median mode diameter of the grown new particles narrowing to 26±2 nm from 13:00 to 15:00, and the two values then slightly decreased till 20:00. However, the grown new particles were still too small to be activated as CCN at 13:00–15:00. From 18:00 to 24:00, the maximum median mode diameter of the grown new particles stopped at 46±2 nm. The calculated κ values were 0.13±0.03 at 0.2 % SS and <0.1 at 0.4 % SS. For CCN activation, particles need to be larger than 100–140 nm. In this case, the increase in N_{ccn} after 13:00 may have been due to the observed growth of pre-existing particles from ~50 nm to particles larger than 100 nm (refer to Fig. 3d). It is possible that less CCN-activated organic vapor was growing on the pre-existing particles since κ values at 0.4 % SS decreased from 0.11 to lower values. However, the increasing size of the pre-existing particles may have canceled out the decreasing effect of κ on N_{ccn}. It is worth noting that even smaller κ values were calculated at 1.0 % SS on 3 July (refer to Fig. S3). Thus, the grown new particles could not have contributed to N_{ccn} at 1.0 % SS.

During the NPF events that occurred from 12–14 July (as shown in Fig. S1a–c), no discernible increase in N_{ccn} at 0.2 % and 0.4 % SS was observed in contrast to the events immediately prior. The 3 day NPF events were often linked to the intrusion of various aerosol plumes. However, based on the combination of lower κ values calculated at 0.2 % and 0.4 % SS and the size of the newly formed particles during these events, it can be inferred that there was likely no net contribution of the grown particles to the observed N_{ccn}.

3.3 Case study with positive contributions to N_{ccn} during NPF events, but not from grown new particles

During NPF events on 30 June and 6 July, an increase in N_{ccn} values at 0.2 % and 0.4 % SS was observed (see Fig. 4a–f). However, the maximum median mode diameter of the newly-formed particles

https://doi.org/10.5194/egusphere-2023-539
Preprint. Discussion started: 27 March 2023

stopped at 19±1 nm on 30 June and 25±1 nm on 6 July (see Fig. 4a–d). On 30 June, the particles grew rapidly before 12:00, stopped growing, and even shrank slightly in the next 11 hours. On 6 July, the particles reached their maximum size at 13:00, stopped growing in the next 3 hours, and disappeared shortly after. The calculated κ values at 0.2 % and 0.4 % SS were smaller than 0.1 on 30 June. On 6 July, the maximum κ values at 0.2 % SS were 0.21±0.02 during 12:00–16:00, and the maximum value at 0.4 % was 0.16 at 16:00. The small size of the newly-formed particles made it unlikely for them to contribute to the increase in N_{ccn} at 0.2 % and 0.4 % SS during the NPF events. Even at 1.0 % SS, the grown new particles were too small to act as CCN due to even smaller κ values (see Fig. S3).

On 30 June, the observed increase in N_{ccn} was partially attributed to the increased number concentration of pre-existing particles. This was demonstrated by a significant correlation between N_{ccn} and $N_{cn>100}$ from 10:00 to 14:00 on that day, with an equation of $N_{ccn} = N_{cn>100} \times 1.42 – 5.6 \times 10^2$, R^2=0.83, and P<0.05 at 0.2 % SS. However, on 3 July, there was no significant correlation between N_{ccn} at 0.2 % SS and $N_{cn>100}$ during the NPF event, implying that the increase in N_{ccn} at 0.2 % and 0.4 % SS was mainly due to the increased κ values of the pre-existing particles (See Fig. 4e).

3.4 Grown new particles unlikely contributed to N_{ccn} at 0.2 % SS on 1 July

In contrast to the seven NPF events discussed above, the newly formed particles experienced continuous growth from <10 nm at 08:30 on 1 July to 65±3 nm at 00:00–04:50 on 2 July (see Fig. 5a). Local meteorological data recorded 0.2 mm rainfall at 04:00–05:00 on 2 July. However, after 04:50 on 2 July, the new particle signal was overwhelmed by the intrusion of aerosol plumes because the N_{cn} varied significantly with an invariant median accumulation mode diameter (see Fig. 2a). Spatial inhomogeneity of the NPF occurrence could not be completely excluded (Zhou et al., 2021). The FR of the NPF event was only 0.82 cm^{-3} s^{-1} on that day, suggesting a weak NPF event. This value ranked lower than the values of 0.06–5.95 cm^{-3} s^{-1} reported in other forest areas (Fiedler et al., 2005; Dal Maso et al., 2005; Han et al., 2013).

During the NPF event on 1 July, a large increase in N_{ccn} was observed at 0.2 % SS (see Fig. 5b). Prior to the NPF event, the N_{ccn} at 0.2 % SS had been 0.6±0.1 $\times 10^3$ cm^{-3} for 4 hours. During the event, there were three stepwise increases: the first stage was 0.8±0.06 $\times 10^3$ cm^{-3}, followed by the second stage which reached 1.3±0.04 $\times 10^3$ cm^{-3} between 13:00 and 19:00. The N_{ccn} then increased to a high level and fluctuated around 1.8±0.2 $\times 10^3$ cm^{-3} (third stage) until the new particle signal disappeared at 04:00–05:00 on 2 July (see Fig. 5b). Overall, the N_{ccn} at 0.2 % SS increased by approximately 200 % during the NPF event compared to the stable values prior to its occurrence.

The maximum κ values at 0.2 % SS were calculated to be 0.30±0.03 from 19:00 on 1 July to 05:00 on 2 July, which was close to the values observed before 06:00 on 29 June and during the non-NPF period observed on 12–14 July. However, the calculated κ values were below 0.2 before 19:00, with CCN-activated sizes larger than 120 nm. The new particles grew with median mode diameters below 35 nm, which were unlikely to contribute to N_{ccn} before 19:00. Therefore, the increased N_{ccn} were likely caused by the pre-existing particles with increasing κ values. The hourly average $N_{cn>100}$ stayed around 1.4±0.02 $\times 10^3$ cm^{-3} from 09:00 to 13:00 and 1.5±0.06 $\times 10^3$ cm^{-3} from 13:00 to 19:00, respectively. The stepwise increase in $N_{cn>100}$ was also likely to reflect the change in pre-existing particle number concentration

https://doi.org/10.5194/egusphere-2023-539
Preprint. Discussion started: 27 March 2023

instead of the continuous growth of newly formed particles and subsequent increase in $N_{cn>100}$.

From 19:00 on 1 July to 05:00 on 2 July, the N_{ccn} at 0.2 % SS were highly correlated with the $N_{cn>100}$, i.e., $N_{ccn} = N_{cn>100} \times 1.01+197$, $R^2=0.89$, $P<0.01$. However, the $N_{cn>100}$ varied around $1.6\pm0.2 \times 10^3$ cm^{-3} during the period and exhibited a stable trend tested by the Mann-Kendall method with P=0.44. The stable trend implied that the contribution from the grown new particles to $N_{cn>100}$ was statistically undetectable. The grown new particles were unlikely to compete with the pre-existing particles to form cloud droplets at 0.2 % SS because of their smaller sizes and lower κ values, despite the possibility of decreased ambient SS with rapid uptake of water vapor on particles (Crumeyrolle et al., 2021; Gong et al., 2023).

3.5 Grown new particles probably contributed to N_{ccn} at 0.4 % and 1.0 % SS on 1 July

Upon analyzing the data at 0.4 % SS on 1–2 July, it was found that the newly grown particles likely contributed significantly to the observed increase in N_{ccn} after 15:00 on 1 July. Prior to this time, although the N_{ccn} at 0.4 % SS had increased, the calculated κ values were below 0.1 for CCN-activated sizes larger than 100 nm. However, the maximum median mode diameter of the newly grown particles was smaller than 27 nm before 15:00. Hence, the increase in N_{ccn} was attributed to the increased κ values of pre-existing particles. After 15:00, the increased κ values led to a smaller CCN-activated size of 67–87 nm at 0.4 % SS. The larger difference in N_{ccn} between 0.2 % and 0.4 % SS was likely due to the increased contribution of the newly grown particles to N_{ccn} at 0.4 % SS (refer to Fig. 5d).

To quantify the contribution of grown new particles to N_{ccn} at 0.4 % SS, we introduced a new term, N_{ccn}, diff, which represents the difference between N_{ccn} at 0.4 % SS and N_{ccn} at 0.2 % SS. We made two assumptions: first, that the N_{ccn}, diff value at 14:00 (386 cm^{-3}) represented the N_{ccn}, diff of pre-existing particles, and second, that the N_{ccn}, diff values of pre-existing particles remained constant after 15:00. Therefore, the difference between N_{ccn}, diff after 15:00 and N_{ccn}, diff at 14:00 represented the net contribution of grown new particles to N_{ccn} at 0.4 % SS. The net contribution of grown new particles was 316 ± 304 cm^{-3} from 15:00 on 1 July to 05:00 on 2 July, accounting for only 12±11 % of N_{ccn} at 0.4 % SS. The maximum net contribution occurred at 16:00 on 1 July and was determined to be 1.0×10^3 cm^{-3}, accounting for 38 % of N_{ccn} at 0.4 % SS. These rough estimates suggest that pre-existing particles were still the major contributor to N_{ccn} at 0.4 % SS, outnumbering new particles.

We used the same method to analyze the contribution of grown new particles to N_{ccn} at 1.0 % SS by calculating $N_{ccn,diff}$, which was the difference between N_{ccn} at 1.0 % and 0.2 % SS (see Fig. 5e). The calculated κ values at 1.0 % SS were lower than those at 0.4 % SS. We assumed that the $N_{ccn,diff}$ at 14:00 (1533 cm^{-3}) represented the substrate constant $N_{ccn,diff}$ of the pre-existing particles after 15:00. However, we observed negative net contributions of the grown new particles to N_{ccn} at 1.0 % SS after 22:00 on July 1, suggesting that the $N_{ccn,diff}$ of pre-existing particles was overestimated. To test the sensitivity of this assumption, we also used the $N_{ccn,diff}$ value at 11:00 (864 cm^{-3}) to represent the $N_{ccn,diff}$ of pre-existing particles after 12:00, and assumed that the $N_{ccn,diff}$ was invariant after 12:00. This analysis indicated that the net contribution of the grown new particles was 769 ± 514 cm^{-3} from 12:00 on 1 July to 05:00 on 2 July, accounting for only 23±12 % of N_{ccn} at 1.0 % SS. The maximum net contribution was 1.9×10^3 cm^{-3} at 18:00 on 1 July, which accounted for 42 % of N_{ccn} at 1.0 % SS. We also observed a minimum

https://doi.org/10.5194/egusphere-2023-539
Preprint. Discussion started: 27 March 2023

contribution of 4 % at 03:00 on 2 July, which was consistent with the disappearance of new particle signals. Thus, using $N_{ccn,diff}$ at 11:00 appeared to be more reasonable than using $N_{ccn,diff}$ at 14:00 to estimate the net contribution of the grown new particles to N_{ccn} at 1.0 % SS.

3.6 Hydrophilic organics dominated the new particle growth, but only NH_4NO_3 formation or hygroscopic organic condensation increased N_{ccn}

Organic species have been widely reported to participate in nucleation and play a significant role in driving the growth of newly formed particles, particularly in forested areas (Makela et al., 2001; Ehn et al., 2007; Smith et al., 2008, 2010; Riipinen et al., 2009). In our study, at 1.0 % SS, the calculated κ values were consistently smaller than 0.13 during all NPF events, with a maximum κ value of 0.08±0.02 from 12:00 on 1 July to 05:00 on 2 July (see Fig. 5c). These results strongly suggest that less hygroscopic organics with low volatility were dominant in the growth of newly formed particles to large sizes.

Sulfuric acid vapor has been widely acknowledged as a crucial factor in the growth of newly formed particles to the size required to become CCN (Birmili et al., 2003; Kulmala et al., 2004; Young et al., 2008; Boy et al., 2005; Kerminen et al., 2018; Chu et al., 2019). Bzdek et al. (2012) found that sulfate contributed to 29–46 % of the total mass in the grown new particles during two campaigns conducted in Delaware, USA. If H_2SO_4 condensation had surpassed organic condensation in shaping pre-existing particles and increasing their κ values on 1 July and 6 July, its amount should have been sufficient to dominate newly formed particles. However, this scenario was practically impossible because the κ values at 1.0 % SS were much lower than those at 0.2 % SS. Nonetheless, κ values did increase during the NPF events on 1 July and 6 July at 0.2 % SS, and were significantly larger than those on other NPF days with $P<0.05$. Although secondary formation of H_2SO_4 and its ammoniated salts on pre-existing particles can occur (Chan and Yao, 2008; Wu et al., 2019), the process was unlikely to be significant in growing newly formed particles based on the low κ values at SS=1.0 %. In fact, the concentrations of SO_4^{2-} in TSP ranged from 0.9 to 4.9 μg m^{-3}, and were not significantly increased on 1 July and 6 July when compared with those on the other six NPF days (See Table 1). These complex results indicate the importance of accurately measuring SO_4^{2-} in different-sized nanometer particles.

NH_4NO_3 formation on newly formed particles was unlikely to occur on those 2 days based on the calculated low κ values at 1.0 % SS. Theoretically, NH_4NO_3 formation requires the product of NH_3 and HNO_3 mixing ratios to be larger than its equilibrium constant plus the Kelvin effect term (Lee et al., 2019; Wang, M. et al., 2020). However, on 1 July and 6 July, NH_4NO_3 formation may have taken over low CCN-activated organic condensation on pre-existing particles larger than 100 nm. For example, the concentrations of NO_3^- were 1.0 μg m^{-3} and 1.8 μg m^{-3} on 1 July and 6 July, respectively, and these values were significantly higher than those on the other six NPF days (0.5–1.0 μg m^{-3}) with $P<0.05$. Additionally, the SOC concentrations of 1.8–2.3 μg m^{-3} on 1 July and 6 July were significantly lower than those of 2.7–4.0 μg m^{-3} on the other 6 days with $P<0.05$. The organic condensation on newly formed and pre-existing particles was likely reduced, indirectly enhancing the NH_4NO_3 formation effects on increasing N_{ccn} and κ values. However, the size-dependent chemical composition of atmospheric particles needs to be confirmed for further analysis.

We further examined four types of secondary organic tracers derived from isoprene, monoterpene,

https://doi.org/10.5194/egusphere-2023-539
Preprint. Discussion started: 27 March 2023

sesquiterpene, and aromatics, as well as primary organic tracers including levoglucosan (LEVO), mannosan, and galactosan, between the two NPF periods (see Tables 1 and S1). However, there was no significant difference in the concentrations of any type of organic tracers between the two NPF periods. It is worth noting that oxalic acid and its salts had high κ values and could be important contributors to increasing κ values at various SS on 1 July and 6 July, particularly during the daytime. However, the measured concentrations of oxalate on those 2 days did not show a significant increase compared to the other days.

We examined the satellite-derived CDNC over the mountain area during and after the NPF day. The values were 169 cm^{-3}, 89 cm^{-3}, and 101 cm^{-3} on 1, 2, and 3 July, respectively (See Fig. 2c). These values were approximately one order of magnitude smaller than the observed N_{ccn} at 0.2 % SS on those 3 days. This large difference between the observed N_{ccn} and satellite-derived CDNC implies that only a small fraction of CCN could competitively capture water vapor to form cloud droplets during the study period (Shen et al., 2018; Jiang et al., 2021; Gong et al., 2023). Moreover, the CDNC during the period from 29 June to 14 July was 120±86 cm^{-3}. The satellite-derived CDNC on 2–3 July were even lower than the average, suggesting that the NPF event was unlikely to have any influence on CNDC.

3.7 Molecular evidence for organics dominating the new particle growth

Figures 6a, b, and S3–S5 compare the static SIMS spectra of atmospheric nanometer particles collected on 30 June and 1 July. On 30 June, the collected particles with diameters of 60 nm (09:20–11:20), 100 nm (07:00–09:00), and 200 nm (13:30–15:30) likely represented the pre-existing particles in the atmosphere, since the maximum median mode diameter of the grown new particles was only 19±1 nm. In the lower mass range of m/z^+ 0–200, the fragments of organics suffered from strong interference from the substrate material (Fig. S4) and were not included in the analysis. The same was true on 1 July. However, the interference from the substrate in the mass range of m/z^+ 200–350 was negligible and was analyzed. Large differences in organic fragment peaks were observed in the mass region of m/z^+ 200–350 between nanometer particles collected on 30 June and 1 July (Fig. 6a, b). Organic peaks, such as m/z^+ 207.047 $C_{14}H_7O_2^+$, 221.158 $C_{14}H_{21}O_2^+$, 265.053 $C_{16}H_9O_4^+$, 267.059 $C_{16}H_{11}O_4^+$, 281.081 $C_{17}H_{13}O_4^+$, 325.013 $C_6H_{13}O_{16}^+$, and 327.018 $C_6H_{15}O_{16}^+$, appeared on particle surfaces with sizes of 60 nm, 100 nm, and 200 nm on 30 June. These organic fragment peaks rarely appeared or had much lower intensities on particle surfaces with sizes of 60 nm (13:00–15:00), 100 nm (18:23–20:23), and 200 nm (06:10–08:10) on 1 July. However, the organic fragment peaks such as m/z^+ 207.047 $C_{14}H_7O_2^+$, 221.158 $C_{14}H_{21}O_2^+$, 281.081 $C_{17}H_{13}O_4^+$, and 327.018 $C_6H_{15}O_{16}^+$ were detected with high intensities on the surface of 30 nm particles collected at 15:10–17:10 on 1 July. The collected particles with a diameter of 30 nm mainly consisted of grown new particles as shown in Fig. 5a. The results suggest that high-molecular-weight organic vapors may preferentially condense on the nanometer particles. However, this was not the case for particles with sizes of 60 nm, 100 nm, and 200 nm on 1 July, when inorganic vapors may have overwhelmingly condensed on the sized particle surfaces and covered up the high-molecular-weight organic fragment signals.

The ToF-SIMS spectral comparisons in the negative ion mode (Figs. S5–S6) yielded similar results, which support the conclusion that the high-molecular-weight organic fragment signals were concealed

https://doi.org/10.5194/egusphere-2023-539
Preprint. Discussion started: 27 March 2023

on the surfaces of the sampled nanometer particles with diameters of 60 nm, 100 nm, and 200 nm on 1 July.

Selected peak spectral PCA of SIMS data was also analyzed (Fig. 7a–c). PC1 was the most important component, explaining 84.5 % of the data, and it separated the 30 nm particles collected on 1 July from the 100 nm and 200 nm particles collected on 30 June, as well as from the 60 nm particles collected on 30 June and 1 July (Fig. 7a). This indicates that PC1 positive loadings shared commonalities for the 30 nm particles on 1 July, and the 100 nm and 200 nm particles on 30 June. The organic fragment signals of the 30 nm particles collected on 1 July were significantly different from those of the larger particles on the same day. Some characteristic peaks were identified as components of organics, such as *m/z*$^+$ 73 $C_4H_9O^+$, 131 $C_8H_5NO^+$, 133 $C_4H_9N_2O_3^+$, 147 $C_6H_{15}SN_2^+$, 161 $C_9H_{21}O_2^+$, 207 $C_{14}H_7O_2^+$, 221 $C_{14}H_{21}O_2^+$, and 281 $C_{17}H_{13}O_4^+$ (Fig. 7b), and they contributed to PC1 positive loadings. These findings support the conclusion that organic vapors drove the condensation growth of 30 nm particles on 30 June and the sized particles on 1 July. Additionally, the PCA results in the negative ion mode showed consistent results with those in positive ion mode (Fig. S7).

4 Summary

During the 2 week field campaign from 29 June to 14 July 2019 at a rural mountain site in NCP, we observed and analyzed eight NPF events. On these NPF days, the total N_{cn} was 8.4±6.1 ×10^3 cm^{-3}, which was substantially higher than the 4.7±2.6 ×10^3 cm^{-3} observed on non-NPF days. However, the N_{ccn} at 0.2 % SS and 0.4 % SS on NPF days was significantly lower than that on non-NPF days, with a p value <0.05. For instance, the N_{ccn} at 0.2 % SS was 1.2±0.7 ×10^3 cm^{-3} on NPF days versus 1.6±0.8 ×10^3 cm^{-3} on non-NPF days. Although the observational data size in this study is small, the comparison suggests that NPF events may not statistically increase N_{ccn} in the middle SS levels. In five of the eight NPF events, we observed either decreases or irregular changes in N_{ccn} with decreasing κ values at various SS. The decreasing κ values were likely attributed to the condensation of hydrophilic organics on newly formed particles and pre-existing particles. Only in one of the eight NPF events did the grown new particles yield detectable net contributions to N_{ccn} at 0.4 % SS and 1.0 % SS with larger sizes of grown new particles and increased κ values. The detectable net contributions accounted for 12±11 % at 0.4 % SS and 23±12 % of N_{ccn} at 1.0 % SS, respectively, during the latter growth period of the NPF event.

During all eight NPF events, the estimated κ values at 1.0 % SS were below 0.13, indicating that hydrophilic organics played a crucial role in the growth of newly formed particles. The estimated κ values at 0.2 % SS were generally smaller than 0.2 and decreased during six of the eight NPF events. In these cases, less hygroscopic organic vapors likely condensed on pre-existing particles, reducing their CCN activation. However, on two of the NPF events (1 July and 6 July), the κ values at 0.2 % SS increased. The significantly higher concentrations of NO_3^- on those days suggested that NH_4NO_3 formation may have contributed to the increased κ values at 0.2 % SS. However, NH_4NO_3 formation on grown new particles was unlikely due to the Kelvin effect.

On 1 July, the SIMS results indicated that high-molecular-weight organic vapors preferentially condensed on the 30 nm particles. In contrast, on >60 nm particle surfaces, inorganic vapors

https://doi.org/10.5194/egusphere-2023-539
Preprint. Discussion started: 27 March 2023

overwhelmingly condensed, concealing the high-molecular-weight organic fragment signals. However, these signals were consistently detected on >60 nm particle surfaces on 30 June due to limited or no condensation of inorganic vapors.

The contribution of NPF events to N_{ccn} needs to be re-evaluated by taking into account the condensation of organic vapors or the formation of NH_4NO_3 on pre-existing particles. Moreover, the N_{ccn} observed in the rural mountain atmosphere was considerably higher than the cloud droplet number concentrations derived from satellites. This suggests that N_{ccn} may be adequate to form cloud droplets in the NCP atmosphere, making the reduced effects of aerosols on ambient SS more crucial.

Data availability. The data of this paper are available upon contact with the authors, Xiaohong Yao (xhyao@ouc.edu.cn) and Xing Wei (17667565924@163.com). The MODIS level-3 daily averaged product (MYD08_D3) used in this paper are available from the Level-1 and Atmosphere Archive and Distribution System (LAADS) Distributed Active Archive Center (DAAC) of NASA (http://ladsweb.nascom.nasa.gov/).

Author contributions. XY (Xiaohong Yao) designed the experiments. XYY (Xiao-Ying Yu) supervised the SIMS analysis, YS conducted the experiments. YS and XW analyzed the data and wrote the paper. XY, XYY, HG and YG provided advice on data processing. XY and XYY revised the original draft of the paper. All authors contributed to editing and improving the paper.

Competing interests. The authors declare that they have no conflict of interest.

Acknowledgement. This research was supported by the National Natural Science Foundation of China (No. 42276036) and Hainan Provincial Natural Science Foundation of China (No. 422MS098). The manuscript preparation for XYY was supported partially by the strategic Laboratory Directed Research and Development (LDRD) of the Physical Sciences Directorate of the Oak Ridge National Laboratory (ORNL).

The authors acknowledge the Beijing Forest Experimental Station of the Institute of Botany, Chinese Academy of Sciences for the help of logistics and permission to access to the site. ChatGPT was used to polish the language paragraph-by-paragraph.

https://doi.org/10.5194/egusphere-2023-539
Preprint. Discussion started: 27 March 2023

References

Ahangar, E. F., Pakbin, P., Hasheminassab, S., Epstein, S. A., Li, X., Polidori, A., and Low, J.: Long-term trends of $PM_{2.5}$ and its carbon content in the south coast air basin: A focus on the impact of wildfires, Atmos. Environ., 255, https://doi.org/10.1016/j.atmosenv.2021.118431, 2021.

Ahmad, I., Mielonen, T., Grosvenor, D. P., Portin, H. J., Arola, A., Mikkonen, S., Kühn, T., Leskinen, A., Joutsensaari, J., Komppula, M., Lehtinen, K. E. J., Laaksonen, A., and Romakkaniemi, S.: Long-term measurements of cloud droplet concentrations and aerosol-cloud interactions in continental boundary layer clouds, Tellus B, 65, https://doi.org/10.3402/tellusb.v65i0.20138, 2013.

Albrecht, B. A.: Aerosols, cloud microphysics, and fractional cloudiness, Science, 245, 1227-1230, https://doi.org/10.1126/science.245.4923.1227, 1989.

Andreae, M. O. and Rosenfeld, D.: Aerosol-cloud-precipitation interactions. Part 1. The nature and sources of cloud-active aerosols, Earth.-Sci. Rev., 89, 13-41, https://doi.org/10.1016/j.earscirev.2008.03.001, 2008.

Bennartz, R.: Global assessment of marine boundary layer cloud droplet number concentration from satellite, J. Geophys. Res., 112, https://doi.org/10.1029/2006jd007547, 2007.

Bennartz, R. and Rausch, J.: Global and regional estimates of warm cloud droplet number concentration based on 13 years of AQUA-MODIS observations, Atmos. Chem. Phys., 17, 9815-9836, https://doi.org/10.5194/acp-2016-1130, 2017.

Birmili, W., Berresheim, H., Plass-Dülmer, C., Elste, T., Gilge, S., Wiedensohler, A., and Uhrner, U.: The Hohenpeissenberg aerosol formation experiment (HAFEX): A long-term study including size-resolved aerosol, H_2SO_4, OH, and monoterpenes measurements, Atmos. Chem. Phys., 3, 361-376, https://doi.org/10.5194/acp-3-361-2003, 2003.

Boreddy, S. K. R. and Kawamura, K.: Investigation on the hygroscopicity of oxalic acid and atmospherically relevant oxalate salts under sub- and supersaturated conditions, Environ. Sci. Process. Impacts., 20, 1069-1080, https://doi.org/10.1039/c8em00053k, 2018.

Bouzidi, H., Fayad, L., Coeur, C., Houzel, N., Petitprez, D., Faccinetto, A., Wu, J., Tomas, A., Ondracek, J., Schwarz, J., Zdimal, V., and Zuend, A.: Hygroscopic growth and CCN activity of secondary organic aerosol produced from dark ozonolysis of gamma-terpinene, Sci. Total. Environ., 817, 153010, https://doi.org/10.1016/j.scitotenv.2022.153010, 2022.

Boy, M., Kulmala, M., Ruuskanen, T. M., Pihlatie, M., Reissell, A., Aalto, P. P., Keronen, P., Dal Maso, M., Hellen, H., Hakola, H., Jansson, R., Hanke, M., and Arnold, F.: Sulphuric acid closure and contribution to nucleation mode particle growth, Atmos. Chem. Phys., 5, 863-878, https://doi.org/10.5194/acp-5-863-2005, 2005.

Bressi, M., Cavalli, F., Putaud, J. P., Fröhlich, R., Petit, J. E., Aas, W., Äijälä, M., Alastuey, A., Allan, J. D., Aurela, M., Berico, M., Bougiatioti, A., Bukowiecki, N., Canonaco, F., Crenn, V., Dusanter, S., Ehn, M., Elsasser, M., Flentje, H., Graf, P., Green, D. C., Heikkinen, L., Hermann, H., Holzinger, R., Hueglin, C., Keernik, H., Kiendler-Scharr, A., Kubelová, L., Lunder, C., Maasikmets, M., Makeš, O., Malaguti, A., Mihalopoulos, N., Nicolas, J. B., O'Dowd, C., Ovadnevaite, J., Petralia, E., Poulain,

https://doi.org/10.5194/egusphere-2023-539
Preprint. Discussion started: 27 March 2023

L., Priestman, M., Riffault, V., Ripoll, A., Schlag, P., Schwarz, J., Sciare, J., Slowik, J., Sosedova, Y., Stavroulas, I., Teinemaa, E., Via, M., Vodička, P., Williams, P. I., Wiedensohler, A., Young, D. E., Zhang, S., Favez, O., Minguillón, M. C., and Prevot, A. S. H.: A European aerosol phenomenology-7: High-time resolution chemical characteristics of submicron particulate matter across Europe, Atmos. Environ., 10, https://doi.org/10.1016/j.aeaoa.2021.100108, 2021.

Bulgin, C. E., Palmer, P. I., Thomas, G. E., Arnold, C. P. G., Campmany, E., Carboni, E., Grainger, R. G., Poulsen, C., Siddans, R., and Lawrence, B. N.: Regional and seasonal variations of the Twomey indirect effect as observed by the ATSR-2 satellite instrument, Geophys. Res. Lett., 35, https://doi.org/10.1029/2007gl031394, 2008.

Bzdek, B. R., Zordan, C. A., Pennington, M. R., Luther, G. W., 3rd, and Johnston, M. V.: Quantitative assessment of the sulfuric acid contribution to new particle growth, Environ. Sci. Technol., 46, 4365-4373, https://doi.org/10.1021/es204556c, 2012.

Cai, M., Tan, H., Chan, C. K., Mochida, M., Hatakeyama, S., Kondo, Y., Schurman, M. I., Xu, H., Li, F., Shimada, K., Li, L., Deng, Y., Yai, H., Matsuki, A., Qin, Y., and Zhao, J.: Comparison of aerosol hygroscopicity, volatility, and chemical composition between a suburban site in the pearl river delta region and a marine site in Okinawa, Aerosol. Air. Qual. Res., 17, 3194-3208, https://doi.org/10.4209/aaqr.2017.01.0020, 2017.

Cao, Z., Zhou, X., Ma, Y., Wang, L., Wu, R., Chen, B., and Wang, W.: The concentrations, formations, relationships and modeling of sulfate, nitrate and ammonium (SNA) aerosols over China, Aerosol. Air. Qual. Res., 17, 84-97, https://doi.org/10.4209/aaqr.2016.01.0020, 2017.

Cerully, K. M., Raatikainen, T., Lance, S., Tkacik, D., Tiitta, P., Petäjä, T., Ehn, M., Kulmala, M., Worsnop, D. R., Laaksonen, A., Smith, J. N., and Nenes, A.: Aerosol hygroscopicity and CCN activation kinetics in a boreal forest environment during the 2007 EUCAARI campaign, Atmos. Chem. Phys., 11, 12369-12386, https://doi.org/10.5194/acp-11-12369-2011, 2011.

Chan, C. K. and Yao, X.: Air pollution in mega cities in China, Atmos. Environ., 42, 1-42, https://doi.org/10.1016/j.atmosenv.2007.09.003, 2008.

Chang, R. Y. W., Abbatt, J. P. D., Boyer, M. C., Chaubey, J. P., and Collins, D. B.: Characterizing the hygroscopicity of growing particles in the Canadian Arctic summer, Atmos. Chem. Phys., 22, 8059-8071, https://doi.org/10.5194/acp-22-8059-2022, 2022.

Che, Y., Zhang, J., Fang, C., Zhou, X., Xue, W., Hu, X., Duan, J., Li, W., Gao, Y., Lu, G., Zhao, D., and Zhao, C.: Aerosol and cloud properties over a coastal area from aircraft observations in Zhejiang, China, Atmos. Environ., 267, https://doi.org/10.1016/j.atmosenv.2021.118771, 2021.

Cheng, W., Weng, L.-T., Li, Y., Lau, A., Chan, C., and Chan, C.-M.: Characterization of size-segregated aerosols using ToF-SIMS imaging and depth profiling, Surf. Interface. Anal., 46, 480-488, https://doi.org/10.1002/sia.5552, 2014.

Cheung, H. C., Chou, C. C.-K., Lee, C. S. L., Kuo, W.-C., and Chang, S.-C.: Hygroscopic properties and cloud condensation nuclei activity of atmospheric aerosols under the influences of Asian continental outflow and new particle formation at a coastal site in eastern Asia, Atmos. Chem. Phys., 20, 5911-5922, https://doi.org/10.5194/acp-20-5911-2020, 2020.

Chu, B., Kerminen, V.-M., Bianchi, F., Yan, C., Petäjä, T., and Kulmala, M.: Atmospheric new particle formation in China, Atmos. Chem. Phys., 19, 115-138, https://doi.org/10.5194/acp-19-115-2019,

https://doi.org/10.5194/egusphere-2023-539
Preprint. Discussion started: 27 March 2023

2019.

Chu, M., Wei, X., Hai, S., Gao, Y., Gao, H., Zhu, Y., Chu, B., Ma, N., Hong, J., Sun, Y., and Yao, X.: Investigating the contribution of grown new particles to cloud condensation nuclei with largely varying pre-existing particles - Part 2: Modeling chemical drivers and 3-D NPF occurrence, 2022.(a companion paper submitted to ACP)

Crippa, M., Canonaco, F., Lanz, V. A., Äijälä, M., Allan, J. D., Carbone, S., Capes, G., Ceburnis, D., Dall'Osto, M., Day, D. A., DeCarlo, P. F., Ehn, M., Eriksson, A., Freney, E., Hildebrandt Ruiz, L., Hillamo, R., Jimenez, J. L., Junninen, H., Kiendler-Scharr, A., Kortelainen, A. M., Kulmala, M., Laaksonen, A., Mensah, A. A., Mohr, C., Nemitz, E., O'Dowd, C., Ovadnevaite, J., Pandis, S. N., Petäjä, T., Poulain, L., Saarikoski, S., Sellegri, K., Swietlicki, E., Tiitta, P., Worsnop, D. R., Baltensperger, U., and Prévôt, A. S. H.: Organic aerosol components derived from 25 AMS data sets across Europe using a consistent ME-2 based source apportionment approach, Atmos. Chem. Phys., 14, 6159-6176, https://doi.org/10.5194/acp-14-6159-2014, 2014.

Crumeyrolle, S., Mensah, A., Khlystov, A., Kos, G., and ten Brink, H.: On the importance of nitrate for the droplet concentration in stratocumulus in the North-Sea region, Atmos. Environ., 252, https://doi.org/10.1016/j.atmosenv.2021.118278, 2021.

Dal Maso, M., Kulmala, M., Riipinen, I., Wagner, R., Hussein, T., Aalto, P., and LehtinenKari, E. J.: Formation and growth of fresh atmospheric aerosols: Eight years of aerosol size distribution data from SMEAR II, Hyytiälä, Finland, Boreal. Environ. Res., 10 (5), 323-336, 2005.

Deng, Y., Kagami, S., Ogawa, S., Kawana, K., Nakayama, T., Kubodera, R., Adachi, K., Hussein, T., Miyazaki, Y., and Mochida, M.: Hygroscopicity of organic aerosols and their contributions to CCN concentrations over a midlatitude forest in Japan, J. Geophys. Res.-Atmos., 123, 9703-9723, https://doi.org/10.1029/2017jd027292, 2018.

Ding, Y., Zhou, Y., Yao, J., Szymanski, C., Fredrickson, J., Shi, L., Cao, B., Zhu, Z., and Yu, X. Y.: In situ molecular imaging of the biofilm and its matrix, Anal. Chem., 88, 11244-11252, https://doi.org/10.1021/acs.analchem.6b03909, 2016.

Ding, Y., Zhou, Y., Yao, J., Xiong, Y., Zhu, Z., and Yu, X. Y.: Molecular evidence of a toxic effect on a biofilm and its matrix, Analyst, 144, 2498-2503, https://doi.org/10.1039/c8an02512f, 2019.

Drugé, T., Nabat, P., Mallet, M., and Somot, S.: Model simulation of ammonium and nitrate aerosols distribution in the Euro-Mediterranean region and their radiative and climatic effects over 1979–2016, Atmos. Chem. Phys., 19, 3707-3731, https://doi.org/10.5194/acp-19-3707-2019, 2019.

Dusek, U., Frank, G. P., Hildebrandt, L., Curtius, J., Schneider, J., Walter, S., Chand, D., Drewnick, F., Hings, S., Jung, D., Borrmann, S., and Andreae, M. O.: Size matters more than chemistry for cloud-nucleating ability of aerosol particles, Science, 312, 1375-1378, https://doi.org/10.1126/science.1125261, 2006.

Dusek, U., Frank, G. P., Curtius, J., Drewnick, F., Schneider, J., Kürten, A., Rose, D., Andreae, M. O., Borrmann, S., and Pöschl, U.: Enhanced organic mass fraction and decreased hygroscopicity of cloud condensation nuclei (CCN) during new particle formation events, Geophys. Res. Lett., 37, L03804, https://doi.org/10.1029/2009gl040930, 2010.

Ehn, M., Petäjä, T., Birmili, W., Junninen, H., Aalto, P., and Kulmala, M.: Non-volatile residuals of newly

https://doi.org/10.5194/egusphere-2023-539
Preprint. Discussion started: 27 March 2023

formed atmospheric particles in the boreal forest, Atmos. Chem. Phys., 7, 677-684, https://doi.org/10.5194/acp-7-677-2007, 2007.

Ehn, M., Thornton, J. A., Kleist, E., Sipila, M., Junninen, H., Pullinen, I., Springer, M., Rubach, F., Tillmann, R., Lee, B., Lopez-Hilfiker, F., Andres, S., Acir, I. H., Rissanen, M., Jokinen, T., Schobesberger, S., Kangasluoma, J., Kontkanen, J., Nieminen, T., Kurten, T., Nielsen, L. B., Jorgensen, S., Kjaergaard, H. G., Canagaratna, M., Maso, M. D., Berndt, T., Petaja, T., Wahner, A., Kerminen, V. M., Kulmala, M., Worsnop, D. R., Wildt, J., and Mentel, T. F.: A large source of low-volatility secondary organic aerosol, Nature, 506, 476-479, https://doi.org/10.1038/nature13032, 2014.

Fang, X., Hu, M., Shang, D., Tan, T., Zhao, G., Zong, T., Tang, L., Ma, X., Yang, X., Dong, H., Yu, X., Chen, S., Li, X., Liu, Y., Wang, H., Gao, Y., Lou, S., Zhao, C., Zeng, L., Lu, K., Zhang, Y., Wu, Z., and Guo, S.: New particle formation and its CCN enhancement in the Yangtze River Delta under the control of continental and marine air masses, Atmos. Environ., 254, https://doi.org/10.1016/j.atmosenv.2021.118400, 2021.

Feng, J., Li, M., Zhang, P., Gong, S., Zhong, M., Wu, M., Zheng, M., Chen, C., Wang, H., and Lou, S.: Investigation of the sources and seasonal variations of secondary organic aerosols in $PM_{2.5}$ in Shanghai with organic tracers, Atmos. Environ., 79, 614-622, https://doi.org/10.1016/j.atmosenv.2013.07.022, 2013.

Fiedler, V., Dal Maso, M., Boy, M., Aufmhoff, H., Hoffmann, J., Schuck, T., Birmili, W., Hanke, M., Uecker, J., Arnold, F., and Kulmala, M.: The contribution of sulphuric acid to atmospheric particle formation and growth: A comparison between boundary layers in Northern and Central Europe, Atmos. Chem. Phys., 5, 1773-1785, https://doi.org/10.5194/acp-5-1773-2005, 2005.

Fisher, G. L., Bruinen, A. L., Ogrinc Potocnik, N., Hammond, J. S., Bryan, S. R., Larson, P. E., and Heeren, R. M.: A new method and mass spectrometer design for tof-sims parallel imaging ms/ms, Anal. Chem., 88, 6433-6440, https://doi.org/10.1021/acs.analchem.6b01022, 2016.

Fu, Y., Zhang, Y., Zhang, F., Chen, J., Zhu, Z., and Yu, X.-Y.: Does interfacial photochemistry play a role in the photolysis of pyruvic acid in water?, Atmos. Environ., 191, 36-45, https://doi.org/10.1016/j.atmosenv.2018.07.061, 2018.

Gao, Y., Zhang, D., Wang, J., Gao, H., and Yao, X.: Variations in N_{cn} and N_{ccn} over marginal seas in China related to marine traffic emissions, new particle formation and aerosol aging, Atmos. Chem. Phys., 20, 9665-9677, https://doi.org/10.5194/acp-20-9665-2020, 2020.

Ge, X., He, Y., Sun, Y., Xu, J., Wang, J., Shen, Y., and Chen, M.: Characteristics and formation mechanisms of fine particulate nitrate in typical urban areas in China, Atmosphere.-Basel., 8, https://doi.org/10.3390/atmos8030062, 2017.

Gong, J., Zhu, Y., Chen, D., Gao, H., Shen, Y., Gao, Y., and Yao, X.: The occurrence of lower-than-expected bulk N_{ccn} values over the marginal seas of China-Implications for competitive activation of marine aerosols, Sci. Total. Environ., 858, 159938, https://doi.org/10.1016/j.scitotenv.2022.159938, 2023.

Gordon, H., Kirkby, J., Baltensperger, U., Bianchi, F., Breitenlechner, M., Curtius, J., Dias, A., Dommen, J., Donahue, N. M., Dunne, E. M., Duplissy, J., Ehrhart, S., Flagan, R. C., Frege, C., Fuchs, C.,

https://doi.org/10.5194/egusphere-2023-539
Preprint. Discussion started: 27 March 2023

Hansel, A., Hoyle, C. R., Kulmala, M., Kürten, A., Lehtipalo, K., Makhmutov, V., Molteni, U., Rissanen, M. P., Stozkhov, Y., Tröstl, J., Tsagkogeorgas, G., Wagner, R., Williamson, C., Wimmer, D., Winkler, P. M., Yan, C., and Carslaw, K. S.: Causes and importance of new particle formation in the present-day and preindustrial atmospheres, J. Geophys. Res.-Atmos., 122, 8739-8760, https://doi.org/10.1002/2017jd026844, 2017.

Grosvenor, D. P., Sourdeval, O., Zuidema, P., Ackerman, A., Alexandrov, M. D., Bennartz, R., Boers, R., Cairns, B., Chiu, J. C., Christensen, M., Deneke, H., Diamond, M., Feingold, G., Fridlind, A., Hunerbein, A., Knist, C., Kollias, P., Marshak, A., McCoy, D., Merk, D., Painemal, D., Rausch, J., Rosenfeld, D., Russchenberg, H., Seifert, P., Sinclair, K., Stier, P., van Diedenhoven, B., Wendisch, M., Werner, F., Wood, R., Zhang, Z., and Quaas, J.: Remote sensing of droplet number concentration in warm clouds: a review of the current state of knowledge and perspectives, Rev. Geophys., 56, 409-453, https://doi.org/10.1029/2017RG000593, 2018.

Gunthe, S. S., King, S. M., Rose, D., Chen, Q., Roldin, P., Farmer, D. K., Jimenez, J. L., Artaxo, P., Andreae, M. O., Martin, S. T., and Pöschl, U.: Cloud condensation nuclei in pristine tropical rainforest air of Amazonia: size-resolved measurements and modeling of atmospheric aerosol composition and CCN activity, Atmos. Chem. Phys., 9, 7551-7575, https://doi.org/10.5194/acp-9-7551-2009, 2009.

Hammer, E., Bukowiecki, N., Gysel, M., Jurányi, Z., Hoyle, C. R., Vogt, R., Baltensperger, U., and Weingartner, E.: Investigation of the effective peak supersaturation for liquid-phase clouds at the high-alpine site Jungfraujoch, Switzerland (3580 m a.s.l.), Atmos. Chem. Phys., 14, 1123-1139, https://doi.org/10.5194/acp-14-1123-2014, 2014.

Han, Y., Iwamoto, Y., Nakayama, T., Kawamura, K., Hussein, T., and Mochida, M.: Observation of new particle formation over a mid-latitude forest facing the North Pacific, Atmos. Environ., 64, 77-84, https://doi.org/10.1016/j.atmosenv.2012.09.036, 2013.

Hirshorn, N. S., Zuromski, L. M., Rapp, C., McCubbin, I., Carrillo-Cardenas, G., Yu, F., and Hallar, A. G.: Seasonal significance of new particle formation impacts on cloud condensation nuclei at a mountaintop location, Atmos. Chem. Phys., 22, 15909-15924, https://doi.org/10.5194/acp-22-15909-2022, 2022.

Hu, Q., Li, K., Zhu, Y., Yu, P., Gao, H., and Yao, X.: Concentration, Size distribution, and formation of trimethylaminium and dimethylaminium ions in atmospheric particles over marginal seas of China, J. Atmos. Sci., 72, 3487-3498, https://doi.org/10.1175/jas-d-14-0393.1, 2015.

Hudson, J. G., Noble, S., and Tabor, S.: Cloud supersaturations from CCN spectra Hoppel minima, J. Geophys. Res.-Atmos., 120, 3436-3452, https://doi.org/10.1002/2014jd022669, 2015.

Hung, H.-M., Lu, W.-J., Chen, W.-N., Chang, C.-C., Chou, C. C. K., and Lin, P.-H.: Enhancement of the hygroscopicity parameter kappa of rural aerosols in northern Taiwan by anthropogenic emissions, Atmos. Environ., 84, 78-87, https://doi.org/10.1016/j.atmosenv.2013.11.032, 2014.

IPCC, 2021: Climate Change 2021: The physical science basis. contribution of working group i to the sixth assessment report of the intergovernmental panel on climate change [Masson-Delmotte, V., P. Zhai, A. Pirani, S. L. Connors, C. Péan, S. Berger, N. Caud, Y. Chen, L. Goldfarb, M. I. Gomis, M. Huang, K. Leitzell, E. Lonnoy, J. B. R. Matthews, T. K. Maycock, T. Waterfield, O. Yelekçi, R. Yu

https://doi.org/10.5194/egusphere-2023-539
Preprint. Discussion started: 27 March 2023

and B. Zhou (eds.)]. Cambridge University Press. In Press. SPM-8, 41.

Iwamoto, Y., Watanabe, A., Kataoka, R., Uematsu, M., and Miura, K.: Aerosol-cloud interaction at the summit of Mt. Fuji, Japan: Factors influencing cloud droplet number concentrations, Appl. Sci.-Basel., 11, https://doi.org/10.3390/app11188439, 2021.

Jiang, S., Zhang, F., Ren, J., Chen, L., Yan, X., Liu, J., Sun, Y., and Li, Z.: Evaluation of the contribution of new particle formation to cloud droplet number concentration in the urban atmosphere, Atmos. Chem. Phys., 21, 14293-14308, https://doi.org/10.5194/acp-21-14293-2021, 2021.

Jones, A. C., Hill, A., Remy, S., Abraham, N. L., Dalvi, M., Hardacre, C., Hewitt, A. J., Johnson, B., Mulcahy, J. P., and Turnock, S. T.: Exploring the sensitivity of atmospheric nitrate concentrations to nitric acid uptake rate using the Met Office's Unified Model, Atmos. Chem. Phys., 21, 15901-15927, https://doi.org/10.5194/acp-21-15901-2021, 2021.

Kalivitis, N., Kerminen, V. M., Kouvarakis, G., Stavroulas, I., Bougiatioti, A., Nenes, A., Manninen, H. E., Petäjä, T., Kulmala, M., and Mihalopoulos, N.: Atmospheric new particle formation as a source of CCN in the eastern Mediterranean marine boundary layer, Atmos. Chem. Phys., 15, 9203-9215, https://doi.org/10.5194/acp-15-9203-2015, 2015.

Kawana, K., Nakayama, T., Kuba, N., and Mochida, M.: Hygroscopicity and cloud condensation nucleus activity of forest aerosol particles during summer in Wakayama, Japan, J. Geophys. Res.-Atmos., 122, 3042-3064, https://doi.org/10.1002/2016jd025660, 2017.

Kerminen, V. M., Paramonov, M., Anttila, T., Riipinen, I., Fountoukis, C., Korhonen, H., Asmi, E., Laakso, L., Lihavainen, H., Swietlicki, E., Svenningsson, B., Asmi, A., Pandis, S. N., Kulmala, M., and Petäjä, T.: Cloud condensation nuclei production associated with atmospheric nucleation: A synthesis based on existing literature and new results, Atmos. Chem. Phys., 12, 12037-12059, https://doi.org/10.5194/acp-12-12037-2012, 2012.

Kerminen, V.-M., Chen, X., Vakkari, V., Petäjä, T., Kulmala, M., and Bianchi, F.: Atmospheric new particle formation and growth: Review of field observations, Environ. Res. Lett., 13, https://doi.org/10.1088/1748-9326/aadf3c, 2018.

Kleindienst, T. E., Jaoui, M., Lewandowski, M., Offenberg, J. H., Lewis, C. W., Bhave, P. V., and Edney, E. O.: Estimates of the contributions of biogenic and anthropogenic hydrocarbons to secondary organic aerosol at a southeastern US location, Atmos. Environ., 41, 8288-8300, https://doi.org/10.1016/j.atmosenv.2007.06.045, 2007.

Kuang, C., McMurry, P. H., and McCormick, A. V.: Determination of cloud condensation nuclei production from measured new particle formation events, Geophys. Res. Lett., 36, https://doi.org/10.1029/2009gl037584, 2009.

Kulmala, M., Vehkamäki, H., Petäjä, T., Dal Maso, M., Lauri, A., Kerminen, V. M., Birmili, W., and McMurry, P. H.: Formation and growth rates of ultrafine atmospheric particles: A review of observations, J. Aerosol. Sci., 35, 143-176, https://doi.org/10.1016/j.jaerosci.2003.10.003, 2004.

Kulmala, M., Petaja, T., Nieminen, T., Sipila, M., Manninen, H. E., Lehtipalo, K., Dal Maso, M., Aalto, P. P., Junninen, H., Paasonen, P., Riipinen, I., Lehtinen, K. E., Laaksonen, A., and Kerminen, V. M.: Measurement of the nucleation of atmospheric aerosol particles, Nat. Protoc., 7, 1651-1667, https://doi.org/10.1038/nprot.2012.091, 2012.

https://doi.org/10.5194/egusphere-2023-539
Preprint. Discussion started: 27 March 2023

Kuwata, M., Kondo, Y., Miyazaki, Y., Komazaki, Y., Kim, J. H., Yum, S. S., Tanimoto, H., and Matsueda, H.: Cloud condensation nuclei activity at Jeju Island, Korea in spring 2005, Atmos. Chem. Phys., 8, 2933-2948, https://doi.org/10.5194/acp-8-2933-2008, 2008.

Lee, S. H., Gordon, H., Yu, H., Lehtipalo, K., Haley, R., Li, Y., and Zhang, R.: New particle formation in the atmosphere: From molecular clusters to global climate, J. Geophys. Res.-Atmos., 124, 7098-7146, https://doi.org/10.1029/2018jd029356, 2019.

Leng, C., Zhang, Q., Tao, J., Zhang, H., Zhang, D., Xu, C., Li, X., Kong, L., Cheng, T., Zhang, R., Yang, X., Chen, J., Qiao, L., Lou, S., Wang, H., and Chen, C.: Impacts of new particle formation on aerosol cloud condensation nuclei (CCN) activity in Shanghai: Case study, Atmos. Chem. Phys., 14, 11353-11365, https://doi.org/10.5194/acp-14-11353-2014, 2014.

Levin, E. J. T., Prenni, A. J., Palm, B. B., Day, D. A., Campuzano-Jost, P., Winkler, P. M., Kreidenweis, S. M., DeMott, P. J., Jimenez, J. L., and Smith, J. N.: Size-resolved aerosol composition and its link to hygroscopicity at a forested site in Colorado, Atmos. Chem. Phys., 14, 2657-2667, https://doi.org/10.5194/acp-14-2657-2014, 2014.

Li, K., Zhu, Y., Gao, H., and Yao, X.: A comparative study of cloud condensation nuclei measured between non-heating and heating periods at a suburb site of Qingdao in the North China, Atmos. Environ., 112, 40-53, https://doi.org/10.1016/j.atmosenv.2015.04.024, 2015.

Li, J., Wang, X., Chen, J., Zhu, C., Li, W., Li, C., Liu, L., Xu, C., Wen, L., Xue, L., Wang, W., Ding, A., and Herrmann, H.: Chemical composition and droplet size distribution of cloud at the summit of Mount Tai, China, Atmos. Chem. Phys., 17, 9885-9896, https://doi.org/10.5194/acp-17-9885-2017, 2017a.

Li, Y., Zhang, F., Li, Z., Sun, L., Wang, Z., Li, P., Sun, Y., Ren, J., Wang, Y., Cribb, M., and Yuan, C.: Influences of aerosol physiochemical properties and new particle formation on CCN activity from observation at a suburban site of China, Atmos. Res., 188, 80-89, https://doi.org/10.1016/j.atmosres.2017.01.009, 2017b.

Li, J., Jian, B., Huang, J., Hu, Y., Zhao, C., Kawamoto, K., Liao, S., and Wu, M.: Long-term variation of cloud droplet number concentrations from space-based Lidar, Remote. Sens. Environ., 213, 144-161, https://doi.org/10.1016/j.rse.2018.05.011, 2018.

Li, J., Li, P., Ren, G., Yuan, L., Li, Y., and Yang, J.: Aircraft measurements of aerosol distribution, warm cloud microphysical properties, and their relationship over the Eastern Loess Plateau in China, Tellus B, 71, https://doi.org/10.1080/16000889.2019.1663994, 2019.

Ma, N., Zhao, C., Tao, J., Wu, Z., Kecorius, S., Wang, Z., Größ, J., Liu, H., Bian, Y., Kuang, Y., Teich, M., Spindler, G., Müller, K., van Pinxteren, D., Herrmann, H., Hu, M., and Wiedensohler, A.: Variation of CCN activity during new particle formation events in the North China Plain, Atmos. Chem. Phys., 16, 8593-8607, https://doi.org/10.5194/acp-16-8593-2016, 2016.

Ma, L., Zhu, Y., Zheng, M., Sun, Y., Huang, L., Liu, X., Gao, Y., Shen, Y., Gao, H., and Yao, X.: Investigating three patterns of new particles growing to the size of cloud condensation nuclei in Beijing's urban atmosphere, Atmos. Chem. Phys., 21, 183-200, https://doi.org/10.5194/acp-21-183-2021, 2021.

Makela, J. M., Yli-Koivisto, S., Hiltunen, V., Seidl, W., Swietlicki, E., Teinila, K., Sillanpaa, M.,

https://doi.org/10.5194/egusphere-2023-539
Preprint. Discussion started: 27 March 2023

Koponen, I. K., Paatero, J., Rosman, K., and Hameri, K.: Chemical composition of aerosol during particle formation events in boreal forest, Tellus B, 53, 380-393, https://doi.org/10.1034/j.1600-0889.2001.530405.x, 2001.

Man, H., Zhu, Y., Ji, F., Yao, X., Lau, N. T., Li, Y., Lee, B. P., and Chan, C. K.: Comparison of daytime and nighttime new particle growth at the HKUST supersite in Hong Kong, Environ. Sci. Technol., 49, 7170-7178, https://doi.org/10.1021/acs.est.5b02143, 2015.

Miao, Q., Zhang, Z., Li, Y., Qin, X., Xu, B., Yuan, Y., and Gao, Z.: Measurement of cloud condensation nuclei (CCN) and CCN closure at Mt. Huang based on hygroscopic growth factors and aerosol number-size distribution, Atmos. Environ., 113, 127-134, https://doi.org/10.1016/j.atmosenv.2015.05.006, 2015.

Park, K. T., Yoon, Y. J., Lee, K., Tunved, P., Krejci, R., Ström, J., Jang, E., Kang, H. J., Jang, S., Park, J., Lee, B. Y., Traversi, R., Becagli, S., and Hermansen, O.: Dimethyl sulfide - induced increase in cloud condensation nuclei in the Arctic atmosphere, Global. Biogeochem. Cy., 35, https://doi.org/10.1029/2021gb006969, 2021.

Petters, M. D. and Kreidenweis, S. M.: A single parameter representation of hygroscopic growth and cloud condensation nucleus activity, Atmos. Chem. Phys., 7, 1961-1971, https://doi.org/10.5194/acp-7-1961-2007, 2007.

Pierce, J. R., Leaitch, W. R., Liggio, J., Westervelt, D. M., Wainwright, C. D., Abbatt, J. P. D., Ahlm, L., Al-Basheer, W., Cziczo, D. J., Hayden, K. L., Lee, A. K. Y., Li, S. M., Russell, L. M., Sjostedt, S. J., Strawbridge, K. B., Travis, M., Vlasenko, A., Wentzell, J. J. B., Wiebe, H. A., Wong, J. P. S., and Macdonald, A. M.: Nucleation and condensational growth to CCN sizes during a sustained pristine biogenic SOA event in a forested mountain valley, Atmos. Chem. Phys., 12, 3147-3163, https://doi.org/10.5194/acp-12-3147-2012, 2012.

Riipinen, I., Manninen, H. E., Yli-Juuti, T., Boy, M., Sipilä, M., Ehn, M., Junninen, H., Petäjä, T., and Kulmala, M.: Applying the condensation Particle Counter Battery (CPCB) to study the water-affinity of freshly-formed 2–9 nm particles in boreal forest, Atmos. Chem. Phys., 9, 3317-3330, https://doi.org/10.5194/acp-9-3317-2009, 2009.

Rodelas, R.R., Perdrix, E., Herbin, B., and Riffault, V.: Characterization and variability of inorganic aerosols and their gaseous precursors at a suburban site in northern France over one year (2015–2016), Atmos. Environ., 200, 142-157, https://doi.org/10.1016/j.atmosenv.2018.11.041, 2019.

Rose, D., Nowak, A., Achtert, P., Wiedensohler, A., Hu, M., Shao, M., Zhang, Y., Andreae, M. O., and Pöschl, U.: Cloud condensation nuclei in polluted air and biomass burning smoke near the mega-city Guangzhou, China-Part 1: Size-resolved measurements and implications for the modeling of aerosol particle hygroscopicity and CCN activity, Atmos. Chem. Phys., 10, 3365-3383, https://doi.org/10.5194/acp-10-3365-2010, 2010.

Rose, D., Gunthe, S. S., Su, H., Garland, R. M., Yang, H., Berghof, M., Cheng, Y. F., Wehner, B., Achtert, P., Nowak, A., Wiedensohler, A., Takegawa, N., Kondo, Y., Hu, M., Zhang, Y., Andreae, M. O., and Pöschl, U.: Cloud condensation nuclei in polluted air and biomass burning smoke near the mega-city Guangzhou, China-Part 2: Size-resolved aerosol chemical composition, diurnal cycles, and externally mixed weakly CCN-active soot particles, Atmos. Chem. Phys., 11, 2817-2836,

https://doi.org/10.5194/egusphere-2023-539
Preprint. Discussion started: 27 March 2023

https://doi.org/10.5194/acp-11-2817-2011, 2011.

Rose, C., Sellegri, K., Moreno, I., Velarde, F., Ramonet, M., Weinhold, K., Krejci, R., Andrade, M., Wiedensohler, A., Ginot, P., and Laj, P.: CCN production by new particle formation in the free troposphere, Atmos. Chem. Phys., 17, 1529-1541, https://doi.org/10.5194/acp-17-1529-2017, 2017.

Sebastian, M., Kanawade, V. P., Soni, V. K., Asmi, E., Westervelt, D. M., Vakkari, V., Hyvärinen, A. P., Pierce, J. R., and Hooda, R. K.: New particle formation and growth to climate-relevant aerosols at a background remote site in the western Himalaya, J. Geophys. Res.-Atmos., 126, https://doi.org/10.1029/2020jd033267, 2021.

Shen, C., Zhao, C., Ma, N., Tao, J., Zhao, G., Yu, Y., and Kuang, Y.: Method to Estimate Water Vapor Supersaturation in the Ambient Activation Process Using Aerosol and Droplet Measurement Data, J. Geophys. Res.-Atmos., 123, https://doi.org/10.1029/2018jd028315, 2018.

Sihto, S. L., Kulmala, M., Kerminen, V. M., Dal Maso, M., Petäjä, T., Riipinen, I., Korhonen, H., Arnold, F., Janson, R., Boy, M., Laaksonen, A., and Lehtinen, K. E. J.: Atmospheric sulphuric acid and aerosol formation: Implications from atmospheric measurements for nucleation and early growth mechanisms, Atmos. Chem. Phys., 6, 4079-4091, https://doi.org/10.5194/acp-6-4079-2006, 2006.

Sihto, S. L., Mikkilä, J., Vanhanen, J., Ehn, M., Liao, L., Lehtipalo, K., Aalto, P. P., Duplissy, J., Petäjä, T., Kerminen, V. M., Boy, M., and Kulmala, M.: Seasonal variation of CCN concentrations and aerosol activation properties in boreal forest, Atmos. Chem. Phys., 11, 13269-13285, https://doi.org/10.5194/acp-11-13269-2011, 2011.

Small, J. D., Chuang, P. Y., Feingold, G., and Jiang, H.: Can aerosol decrease cloud lifetime? Geophys. Res. Lett., 36, https://doi.org/10.1029/2009gl038888, 2009.

Smith, J. N., Dunn, M. J., VanReken, T. M., Iida, K., Stolzenburg, M. R., McMurry, P. H., and Huey, L. G.: Chemical composition of atmospheric nanoparticles formed from nucleation in Tecamac, Mexico: Evidence for an important role for organic species in nanoparticle growth, Geophys. Res. Lett., 35, https://doi.org/10.1029/2007gl032523, 2008.

Smith, J. N., Barsanti, K. C., Friedli, H. R., Ehn, M., Kulmala, M., Collins, D. R., Scheckman, J. H., Williams, B. J., and McMurry, P. H.: Observations of ammonium salts in atmospheric nanoparticles and possible climatic implications, P. Natl. Acad. Sci. USA, 107, 6634-6639, https://doi.org/10.1073/pnas.0912127107, 2010.

Sotiropoulou, R. E. P., Tagaris, E., Pilinis, C., Anttila, T., and Kulmala, M.: Modeling new particle formation during air pollution episodes: Impacts on aerosol and cloud condensation nuclei, Aerosol. Sci. Tech., 40, 557-572, https://doi.org/10.1080/02786820600714346, 2006.

Sui, X., Zhou, Y., Zhang, F., Zhang, Y., Chen, J., Zhu, Z., and Yu, X. Y.: ToF-SIMS characterization of glyoxal surface oxidation products by hydrogen peroxide: A comparison between dry and liquid samples, Surf. Interface. Anal., 50, 927-938, https://doi.org/10.1002/sia.6334, 2017.

Sullivan, R. C., Crippa, P., Matsui, H., Leung, L. R., Zhao, C., Thota, A., and Pryor, S. C.: New particle formation leads to cloud dimming, npj. Clim. Atmos. Sci., 1, https://doi.org/10.1038/s41612-018-0019-7, 2018.

Teng, X., Hu, Q., Zhang, L., Qi, J., Shi, J., Xie, H., Gao, H., and Yao, X.: Identification of Major Sources

https://doi.org/10.5194/egusphere-2023-539
Preprint. Discussion started: 27 March 2023

of Atmospheric NH_3 in an Urban Environment in Northern China During Wintertime, Environ. Sci. Technol., 51, 6839-6848, https://doi.org/10.1021/acs.est.7b00328, 2017.

Tröstl, J., Herrmann, E., Frege, C., Bianchi, F., Molteni, U., Bukowiecki, N., Hoyle, C. R., Steinbacher, M., Weingartner, E., Dommen, J., Gysel, M., and Baltensperger, U.: Contribution of new particle formation to the total aerosol concentration at the high-altitude site Jungfraujoch (3580 m asl, Switzerland), J. Geophys. Res.-Atmos., 121, https://doi.org/10.1002/2015jd024637, 2016.

Twohy, C. H.: Evaluation of the aerosol indirect effect in marine stratocumulus clouds: Droplet number, size, liquid water path, and radiative impact, J. Geophys. Res., 110, https://doi.org/10.1029/2004jd005116, 2005.

Twomey, S.: The influence of pollution on the shortwave albedo of clouds, J. Atmos. Sci., 34, 1149-1152, https://doi.org/10.1175/1520-0469(1977)034<1149:Tiopot>2.0.Co;2, 1977.

Vakkari, V., Tiitta, P., Jaars, K., Croteau, P., Beukes, J. P., Josipovic, M., Kerminen, V. M., Kulmala, M., Venter, A. D., Zyl, P. G., Worsnop, D. R., and Laakso, L.: Reevaluating the contribution of sulfuric acid and the origin of organic compounds in atmospheric nanoparticle growth, Geophys. Res. Lett., 42, https://doi.org/10.1002/2015gl066459, 2015.

Wan, Y., Huang, X., Jiang, B., Kuang, B., Lin, M., Xia, D., Liao, Y., Chen, J., Yu, J. Z., and Yu, H.: Probing key organic substances driving new particle growth initiated by iodine nucleation in coastal atmosphere, Atmos. Chem. Phys., 20, 9821-9835, https://doi.org/10.5194/acp-20-9821-2020, 2020.

Wang, J., Shen, Y., Li, K., Gao, Y., Gao, H., and Yao, X.: Nucleation-mode particle pool and large increases in N_{cn} and N_{ccn} observed over the northwestern Pacific Ocean in the spring of 2014, Atmos. Chem. Phys., 19, 8845-8861, https://doi.org/10.5194/acp-19-8845-2019, 2019.

Wang, M., Kong, W., Marten, R., He, X. C., Chen, D., Pfeifer, J., Heitto, A., Kontkanen, J., Dada, L., Kurten, A., Yli-Juuti, T., Manninen, H. E., Amanatidis, S., Amorim, A., Baalbaki, R., Baccarini, A., Bell, D. M., Bertozzi, B., Brakling, S., Brilke, S., Murillo, L. C., Chiu, R., Chu, B., De Menezes, L. P., Duplissy, J., Finkenzeller, H., Carracedo, L. G., Granzin, M., Guida, R., Hansel, A., Hofbauer, V., Krechmer, J., Lehtipalo, K., Lamkaddam, H., Lampimaki, M., Lee, C. P., Makhmutov, V., Marie, G., Mathot, S., Mauldin, R. L., Mentler, B., Muller, T., Onnela, A., Partoll, E., Petaja, T., Philippov, M., Pospisilova, V., Ranjithkumar, A., Rissanen, M., Rorup, B., Scholz, W., Shen, J., Simon, M., Sipila, M., Steiner, G., Stolzenburg, D., Tham, Y. J., Tome, A., Wagner, A. C., Wang, D. S., Wang, Y., Weber, S. K., Winkler, P. M., Wlasits, P. J., Wu, Y., Xiao, M., Ye, Q., Zauner-Wieczorek, M., Zhou, X., Volkamer, R., Riipinen, I., Dommen, J., Curtius, J., Baltensperger, U., Kulmala, M., Worsnop, D. R., Kribi, J., Seinfeld, J. H., El-Haddad, I., Flagman, R. C., and Donahue, N. M.: Rapid growth of new atmospheric particles by nitric acid and ammonia condensation, Nature, 581, 184-189, https://doi.org/10.1038/s41586-020-2270-4, 2020.

Whitby, K. T.: The physical characteristics of sulfur aerosols, Atmos. Environ. (1967), 12, 135-159, http://dx.doi.org/10.1016/0004-6981(78)90196-8, 1978.

Wiedensohler, A., Cheng, Y. F., Nowak, A., Wehner, B., Achtert, P., Berghof, M., Birmili, W., Wu, Z. J., Hu, M., Zhu, T., Takegawa, N., Kita, K., Kondo, Y., Lou, S. R., Hofzumahaus, A., Holland, F., Wahner, A., Gunthe, S. S., Rose, D., Su, H., and Pöschl, U.: Rapid aerosol particle growth and increase of cloud condensation nucleus activity by secondary aerosol formation and condensation:

https://doi.org/10.5194/egusphere-2023-539
Preprint. Discussion started: 27 March 2023

A case study for regional air pollution in northeastern China, J. Geophys. Res., 114, https://doi.org/10.1029/2008jd010884, 2009.

Williamson, C. J., Kupc, A., Axisa, D., Bilsback, K. R., Bui, T., Campuzano-Jost, P., Dollner, M., Froyd, K. D., Hodshire, A. L., Jimenez, J. L., Kodros, J. K., Luo, G., Murphy, D. M., Nault, B. A., Ray, E. A., Weinzierl, B., Wilson, J. C., Yu, F., Yu, P., Pierce, J. R., and Brock, C. A.: A large source of cloud condensation nuclei from new particle formation in the tropics, Nature, 574, 399-403, https://doi.org/10.1038/s41586-019-1638-9, 2019.

Wu, Z., Birmili, W., Poulain, L., Wang, Z., Merkel, M., Fahlbusch, B., van Pinxteren, D., Herrmann, H., and Wiedensohler, A.: Particle hygroscopicity during atmospheric new particle formation events: Implications for the chemical species contributing to particle growth, Atmos. Chem. Phys., 13, 6637-6646, https://doi.org/10.5194/acp-13-6637-2013, 2013.

Wu, P., Huang, X., Zhang, J., Luo, B., Luo, J., Song, H., Zhang, W., Rao, Z., Feng, Y., and Zhang, J.: Characteristics and formation mechanisms of autumn haze pollution in Chengdu based on high time-resolved water-soluble ion analysis, Environ. Sci. Pollut. R, 26, 2649-2661, https://doi.org/10.1007/s11356-018-3630-6, 2019.

Yang, J., Li, J., Li, P., Sun, G., Cai, Z., Yang, X., Cui, C., Dong, X., Xi, B., Wan, R., Wang, B., and Zhou, Z.: Spatial distribution and impacts of aerosols on clouds under meiyu frontal weather background over central China based on aircraft observations, J. Geophys. Res.-Atmos., 125, https://doi.org/10.1029/2019jd031915, 2020.

Yao, X., Lau, N. T., Fang, M. and Chan, C. K.: Real-Time Observation of the Transformation of Ultrafine Atmospheric Particle Modes, Atmos. Chem. Phys., 8, 4997-5016, https://doi.org/10.1080/02786820500295248, 2007.

Yao, X., Choi, M. Y., Lau, N. T., Lau, A. P. S., Chan, C. K., and Fang, M.: Growth and shrinkage of new particles in the atmosphere in Hong Kong, Aerosol. Sci. Tech., 44, 639-650, https://doi.org/10.1080/02786826.2010.482576, 2010.

Young, L. H., Benson, D. R., Kameel, F. R., Pierce, J. R., Junninen, H., Kulmala, M., and Lee, S. H.: Laboratory studies of H_2SO_4/H_2O binary homogeneous nucleation from the SO_2+OH reaction: Evaluation of the experimental setup and preliminary results, Atmos. Chem. Phys., 8, 4997-5016, https://doi.org/10.5194/acp-8-4997-2008, 2008.

Yu, F. and Luo, G.: Simulation of particle size distribution with a global aerosol model: Contribution of nucleation to aerosol and CCN number concentrations, Atmos. Chem. Phys., 9, 7691-7710, https://doi.org/10.5194/acp-9-7691-2009, 2009.

Yu, F., Luo, G., Nair, A. A., Schwab, J. J., Sherman, J. P., and Zhang, Y.: Wintertime new particle formation and its contribution to cloud condensation nuclei in the Northeastern United States, Atmos. Chem. Phys., 20, 2591-2601, https://doi.org/10.5194/acp-20-2591-2020, 2020.

Yu, X. Y., Cary, R. A., and Laulainen, N. S.: Primary and secondary organic carbon downwind of Mexico City, Atmos. Chem. Phys., 9, 6793-6814, https://doi.org/10.5194/acp-9-6793-2009, 2009.

Yue, D. L., Hu, M., Zhang, R. Y., Wu, Z. J., Su, H., Wang, Z. B., Peng, J. F., He, L. Y., Huang, X. F., Gong, Y. G., and Wiedensohler, A.: Potential contribution of new particle formation to cloud condensation nuclei in Beijing, Atmos. Environ., 45, 6070-6077,

https://doi.org/10.5194/egusphere-2023-539
Preprint. Discussion started: 27 March 2023

https://doi.org/10.1016/j.atmosenv.2011.07.037, 2011.

Zaveri, R. A., Easter, R. C., Singh, B., Wang, H., Lu, Z., Tilmes, S., Emmons, L. K., Vitt, F., Zhang, R., Liu, X., Ghan, S. J., and Rasch, P. J.: Development and evaluation of chemistry-aerosol-climate model CAM5-Chem-MAM7-MOSAIC: global atmospheric distribution and radiative effects of nitrate aerosol, J. Adv. Model. Earth. Sy., 13, e2020MS002346, https://doi.org/10.1029/2020MS002346, 2021.

Zhang, F., Yu, X., Chen, J., Zhu, Z., and Yu, X.-Y.: Dark air-liquid interfacial chemistry of glyoxal and hydrogen peroxide, npj. Clim. Atmos. Sci., 2, https://doi.org/10.1038/s41612-019-0085-5, 2019.

Zhou, Y., Hakala, S., Yan, C., Gao, Y., Yao, X., Chu, B., Chan, T., Kangasluoma, J., Gani, S., Kontkanen, J., Paasonen, P., Liu, Y., Petäjä, T., Kulmala, M., and Dada, L.: Measurement report: New particle formation characteristics at an urban and a mountain station in northern China, Atmos. Chem. Phys., 21, 17885-17906, https://doi.org/10.5194/acp-21-17885-2021, 2021.

Zhu, Y., Sabaliauskas, K., Liu, X., Meng, H., Gao, H., Jeong, C.-H., Evans, G. J., and Yao, X.: Comparative analysis of new particle formation events in less and severely polluted urban atmosphere, Atmos. Environ., 98, 655-664, https://doi.org/10.1016/j.atmosenv.2014.09.043, 2014.

Zhu, J., Penner, J. E., Yu, F., Sillman, S., Andreae, M. O., and Coe, H.: Decrease in radiative forcing by organic aerosol nucleation, climate, and land use change, Nat. Commun., 10, 423, https://doi.org/10.1038/s41467-019-08407-7, 2019a.

Zhu, Y., Li, K., Shen, Y., Gao, Y., Liu, X., Yu, Y., Gao, H., and Yao, X.: New particle formation in the marine atmosphere during seven cruise campaigns, Atmos. Chem. Phys., 19, 89-113, https://doi.org/10.5194/acp-19-89-2019, 2019b.

Zhu, Y., Shen, Y., Li, K., Meng, H., Sun, Y., Yao, X., Gao, H., Xue, L., and Wang, W.: Investigation of particle number concentrations and new particle formation with largely reduced air pollutant emissions at a coastal semi-urban site in northern China, J. Geophys. Res.-Atmos., 126, https://doi.org/10.1029/2021jd035419, 2021.

Zimmerman, N., Jeong, C.-H., Wang, J. M., Ramos, M., Wallace, J. S., and Evans, G. J.: A source-independent empirical correction procedure for the fast mobility and engine exhaust particle sizers, Atmos. Environ., 100, 178-184, https://doi.org/10.1016/j.atmosenv.2014.10.054, 2015.

https://doi.org/10.5194/egusphere-2023-539
Preprint. Discussion started: 27 March 2023

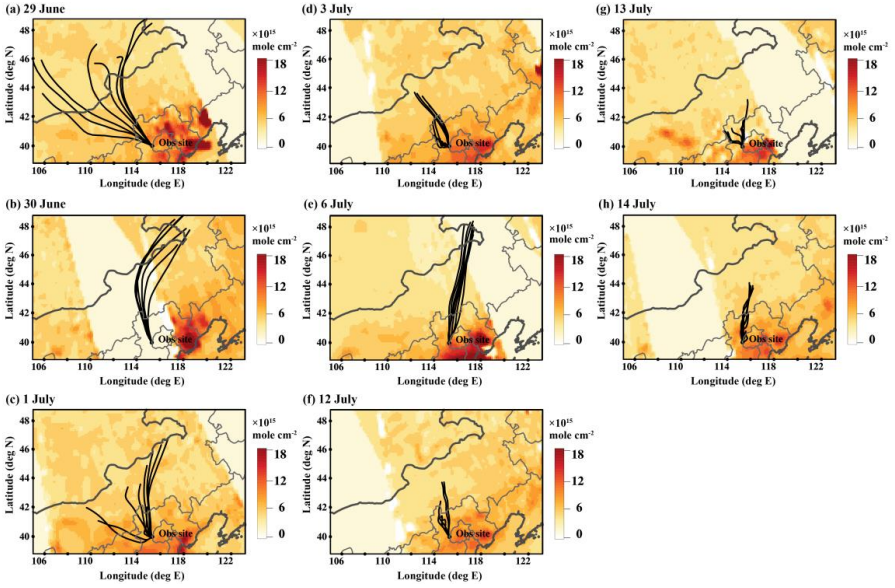

Figure 1. Satellite NO_2 column density over the observational site and surrounding areas and air mass back trajectories during eight NPF event days in June–July 2019 (a–f correspond to the NO_2 column density recorded on 29 June, 30 June, 1 July, 3 July, 6 July, 12–14 July, respectively).

https://doi.org/10.5194/egusphere-2023-539
Preprint. Discussion started: 27 March 2023

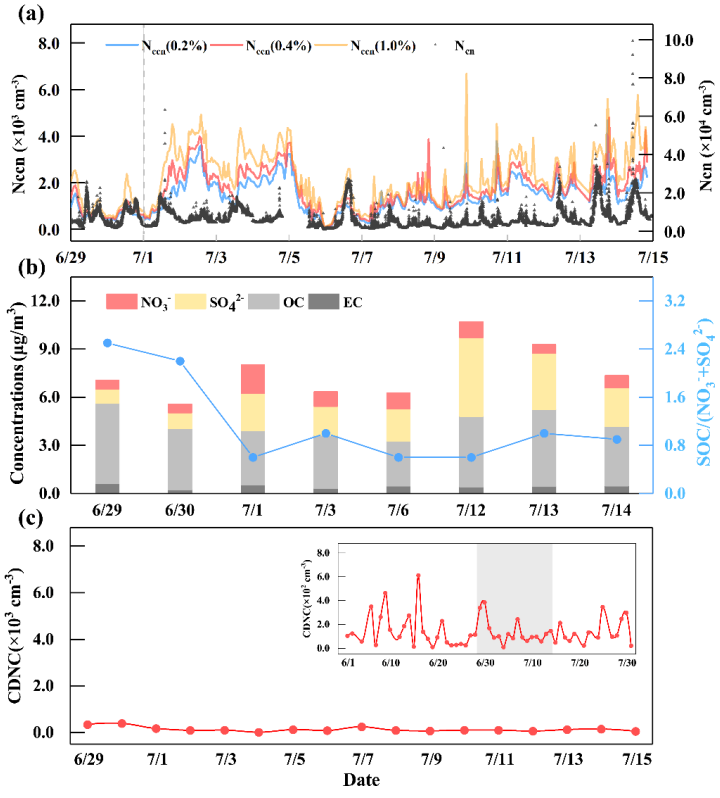

Figure 2. Temporal variations in N_{ccn} at 0.2 %, 0.4 % and 1.0 % SS, N_{cn} (a); daily average concentrations of chemical components in TSP and related ratios of SOC/(NO_3^-+SO_4^{2-}) (b); Satellite-derived CDNC from June 29 to 15 July 2019 (CNDC in June to July were superimposed in c) (c).

https://doi.org/10.5194/egusphere-2023-539
Preprint. Discussion started: 27 March 2023

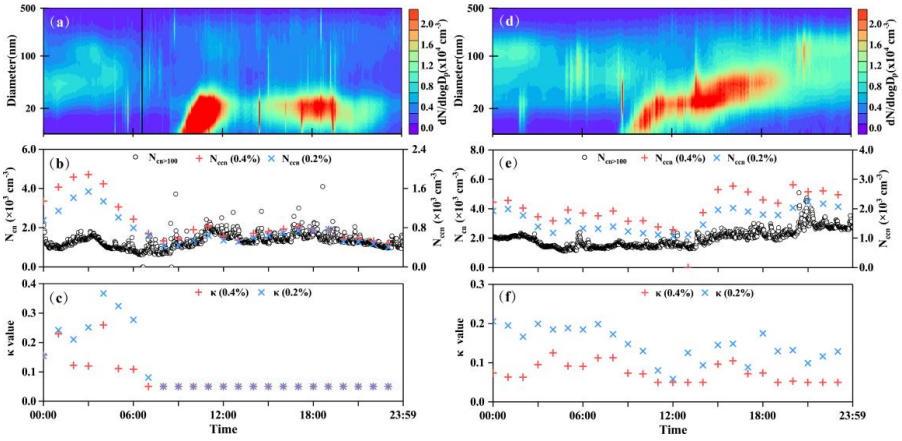

Figure 3. The contour plots of particle number size distribution, and time series of $N_{cn>100}$, N_{ccn} and κ values at 0.2 % and 0.4 % SS on 29 June and 3 July (a: contour plots of PNSD on 29 June; b: time series of $N_{cn>100}$ and N_{ccn} at 0.2 % and 0.4 % SS on 29 June; c: κ values at 0.2 % and 0.4 % SS on 29 June; d–f same as a–c except on 3 July).

https://doi.org/10.5194/egusphere-2023-539
Preprint. Discussion started: 27 March 2023

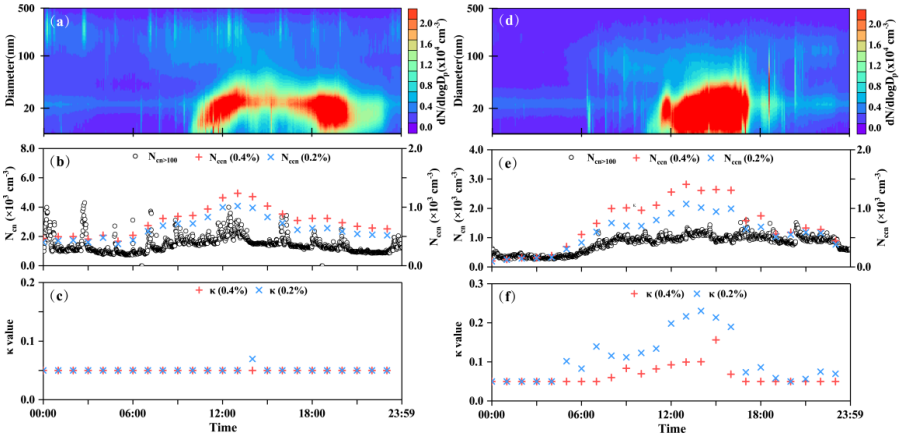

Figure 4. The same as Figure 3 except on 30 June and 6 July.

https://doi.org/10.5194/egusphere-2023-539
Preprint. Discussion started: 27 March 2023

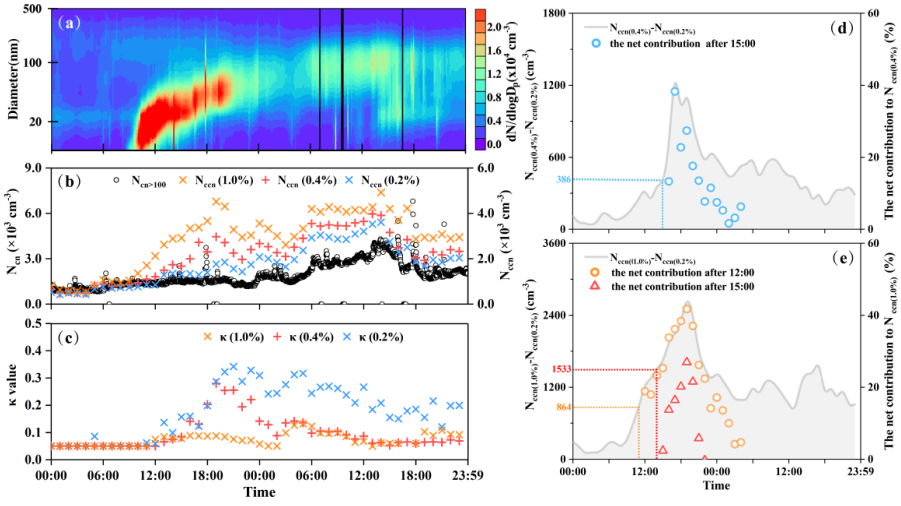

Figure 5. The contour plots of particle number size distribution (a); Times series of N_{ccn} at 0.2 %, 0.4 % and 1.0 % SS and $N_{cn>100}$ (b); Time series of κ values at 0.2 %, 0.4 % and 1.0 % SS (c); Time series of ($N_{ccn(0.4\%)}$–$N_{ccn(0.2\%)}$) and ratios of ($N_{ccn(0.4\%)}$–$N_{ccn(0.2\%)}$)/$N_{ccn(0.4\%)}$ (d); Time series of ($N_{ccn(1.0\%)}$–$N_{ccn(0.2\%)}$) ratios of ($N_{ccn(1.0\%)}$–$N_{ccn(0.2\%)}$)/$N_{ccn(1.0\%)}$ (e) on 1–2 July.

https://doi.org/10.5194/egusphere-2023-539
Preprint. Discussion started: 27 March 2023

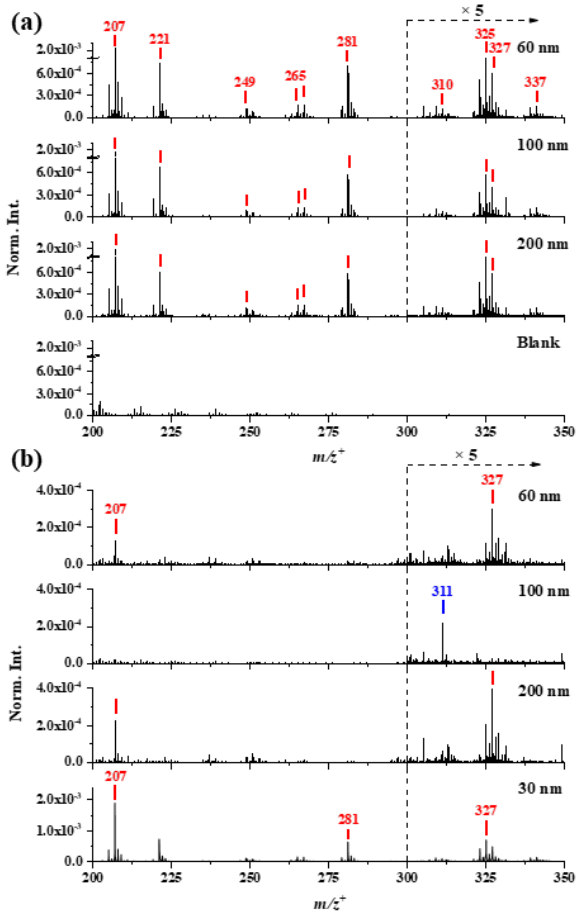

Figure 6. ToF-SIMS spectral comparison of atmospheric nanometer particles collected on 30 June (a) and 1 July 2019 (b) in the positive ion mode (m/z^+ 200−350).

https://doi.org/10.5194/egusphere-2023-539
Preprint. Discussion started: 27 March 2023

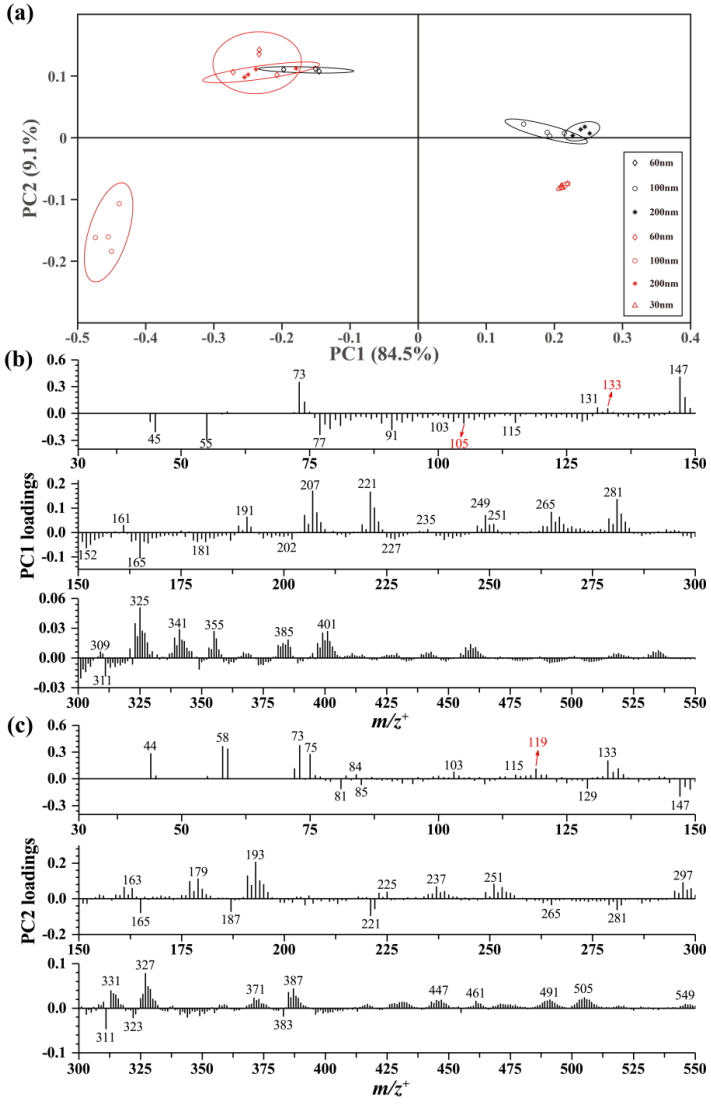

Figure 7. ToF-SIMS selected peak spectral PCA results of 60 nm, 100 nm, and 200 nm particles on 30 June (gray markers) as well as 30 nm, 60 nm, 100 nm, and 200 nm particles on 1 July (red markers) in the positive mode: Scores plots of PC1 vs. PC2 (a), PC1 loadings plots in m/z^+ 30–550 (b), and PC2 loading plots in m/z^+ 30–550 (c). Peaks are labelled in their center masses.

https://doi.org/10.5194/egusphere-2023-539
Preprint. Discussion started: 27 March 2023

Table 1. Concentrations of SOA tracers, OC, EC, and ions in TSP on NPF days

Chemical components	29 June	30 June	1 July	3 July	6 July	12 July	13 July	14 July
	Isoprene SOA tracers (ng m^{-3})							
2-methylglyceric acid	0.04	0.44	0.65	1.9	0.21	0.17	6.2	1.4
cis-2-Methyl-1,3,4-trihydroxy-1-butene	0.12	1.0	0.59	1.2	0.98	2.5	36	39
3-Methyl-2,3,4-trihydroxy-1-butene	0.24	1.61	0.50	0.52	0.31	1.10	16.39	23
trans-2-Methyl-1,3,4-trihydroxy-1-butene	0.15	0.73	0.36	0.02	0.16	1.2	17	13
2-methylthreitol	1.2	11	5.8	2.3	5.2	0.72	32	1.0×10^2
2-methylerythritol	2.9	22	17	7.6	15	1.3	75	2.2×10^2
Sum of them	4.6	37	25	14	22	7.0	1.8×10^2	4.0×10^2
	Biomass burning tracer (ng m^{-3}), OC and EC (μg m^{-3})							
levoglucosan	2.6	11	0.21	2.2	0.44	0.16	0.84	0.72
OC	5.0	3.8	3.4	3.3	2.8	4.4	4.9	3.7
EC	0.61	0.23	0.53	0.32	0.47	0.41	0.43	0.47
	Water-soluble inorganic and organic ions (μg m^{-3})							
NO_3^-	0.57	0.54	1.8	0.92	1.0	0.99	0.55	0.78
SO_4^{2-}	0.89	1.1	2.3	1.8	2.0	4.9	3.5	2.4
Oxalate	0.08	0.08	0.16	0.15	0.11	0.15	0.17	0.18